NUCLEAR DATA AND MEASUREMENTS SERIES

ANL/NDM-155

FAST-NEUTRON SCATTERING FROM ELEMENTAL RHENIUM*

by
Alan B. Smith

August 2003

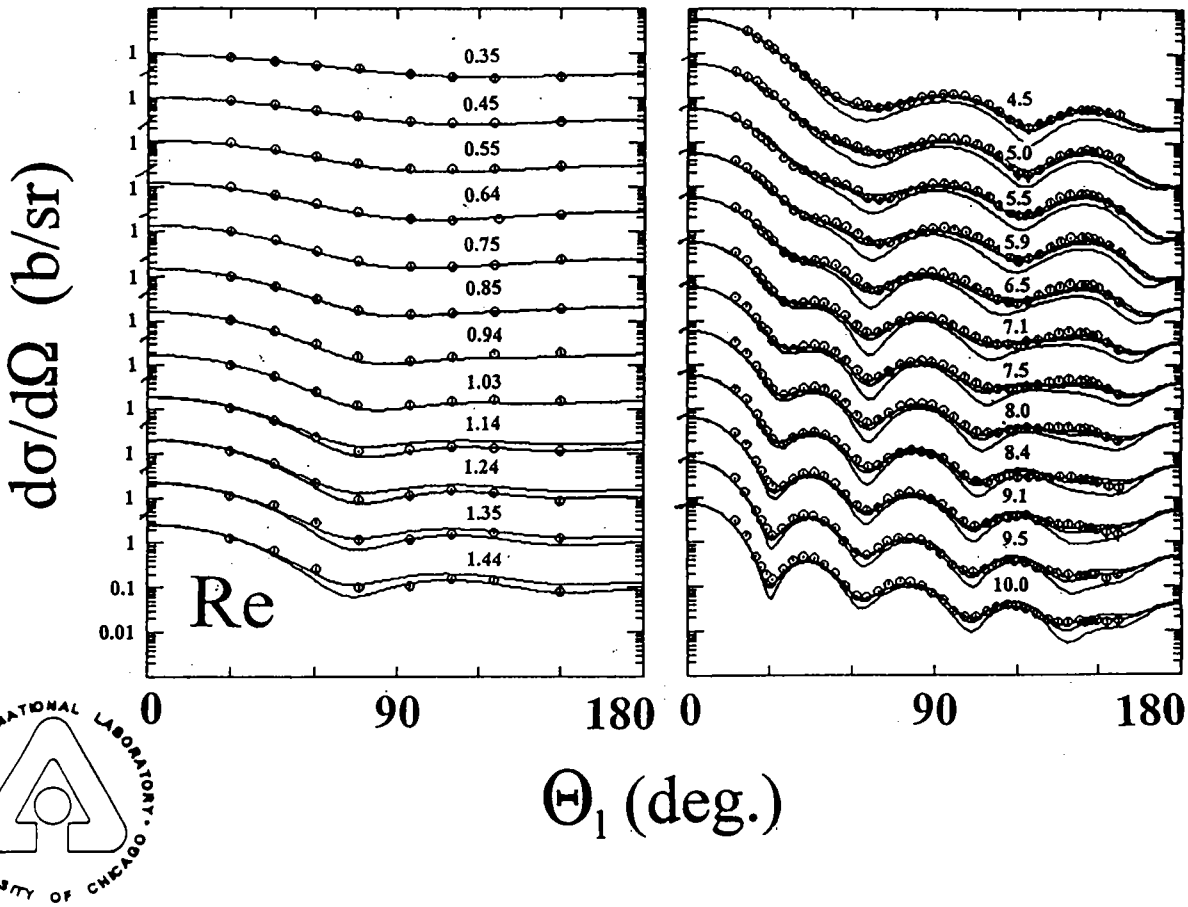

ARGONNE NATIONAL LABORATORY, ARGONNE, ILLINOIS
Operated by THE UNIVERSITY OF CHICAGO
for the U. S. DEPARTMENT OF ENERGY
under Contract W-31-109-Eng-38

Nuclear Data and Measurement Series

Reports in the Argonne National Laboratory Nuclear Data and Measurement Series present results of studies in the field of microscopic nuclear data. The primary objective of the series is the dissemination of information in the comprehensive form required for nuclear technology applications. This series is devoted to: a) measured microscopic nuclear parameters, b) experimental techniques and facilities employed in measurements, c) the analysis, correlation and interpretation of nuclear data, and d) the compilation and evaluation of nuclear data. Contributions to this Series are reviewed to assure technical competence and, unless otherwise stated, the contents can be formally referenced. This Series does not supplant formal journal publication, but it does provide the more extensive information required for technological applications (e.g., tabulated numerical data) in a timely manner.

Argonne National Laboratory, with facilities in the states of Illinois and Idaho, is owned by the United States Government, and operated by the University of Chicago under provisions of a contract with the Department of Energy.

Disclaimer

This report is available electronically at <http://www.doe.gov/bridge>. It is also available for a processing fee to the U. S. Department of Energy and its contractors in paper form from:-

U. S. Department of Energy
Office of Scientific and Technical information
P. O. Box 62
Oak Ridge, TN 37831-0062 Fax: (865) 576-5728
Phone: (865) 576-8401 E-mail: <reports@adonis.osti.gov>

Publications in the ANL/NDM Series

A listing of recent issues in this series is given below. Issues and/or titles prior to ANL/NDM-130 can be obtained from the National Technical Information Service, U. S. Department of Commerce, Technology Administration, Springfield, VA 22161, or by contacting the author of this report at the Nuclear Engineering Division, Argonne National Laboratory, 9700 South Cass Avenue, Argonne, IL 60439 (USA). In addition, the entire report series can be found on the Internet at the following URL: <http://www.td.anl.gov/reports/ANLNDMReports.html>, including abstracts, complete reports, and associated computer programs.

A. B. Smith and P. T. Guenther
Fast-neutron interaction with the fission product ^{103}Rh
ANL/NDM-130, September 1993

A. B. Smith and P. T. Guenther
Fast-neutron scattering from vibrational Palladium nuclei
ANL/NDM-131, October 1993

A. B. Smith
Neutron interaction with doubly-magic ^{40}Ca
ANL/NDM-132, November 1993

A. B. Smith
Fast-neutron scattering at Z=50:- Tin
ANL/NDM-133, September 1994

A. B. Smith, S. Chiba and J. W. Meadows
An evaluated neutronic data file for elemental Zirconium
ANL/NDM-134, September 1994

A. B. Smith and S. Chiba
Neutron scattering from Uranium and Thorium
ANL/NDM-135, February 1995

A. B. Smith
Neutron scattering and models:- Iron
ANL/NDM-136, August 1995

A. B. Smith
Neutron scattering and models:- Silver
ANL/NDM-137, July 1996

A. B. Smith and D. Schmidt
Neutron scattering and models:- Chromium
ANL/NDM-138 June 1996

W. P. Poenitz and S. E. Aumeier
The simultaneous evaluation of the standards and other cross sections of importance for technology
ANL/NDM-139, September 1997

D. L. Smith and J. T. Daly
A compilation of information on the ^{31}P(p,gamma)^{32}S reaction and properties of excited

levels in ^{32}S
ANL/NDM-140, November 2000

A. B. Smith
Neutron scattering and models:- Titanium
ANL/NDM-141, July 1997

A. B. Smith
Neutron scattering and models:- Molybdenum
ANL/NDM-142, July 1999

R. E. Miller and D. L. Smith
Compilation of information on the $^{31}P(p,gamma)^{33}Cl$ reaction and properties of excited levels in ^{33}Cl
ANL/NDM-143, July 1997

R. E. Miller and D. L. Smith
A compilation of information on the $^{31}P(p,gamma)^{28}Si$ reaction and properties of the excited levels in ^{28}Si
ANL/NDM-144, November 1997

R. D. Lawson and A. B. Smith
ABAREX, a neutron spherical optical-statistical model code:- A user's manual
ANL/NDM-145, June 1999

R. T. Klann and W. P. Poenitz
Non-destructive assay of EBR-II blanket elements using resonance transmission analysis
ANL/NDM-146, 1998

A. B. Smith
ELEMENTAL-ABAREX:- A user's manual
ANL/NDM-147, June 1999

D. G. Naberejnev and D. L. Smith
A method to construct covariance files in ENDF/B formats for critical safety applications
ANL/NDM-148, June 1999

A. B. Smith
Neutrons and antimony:- physical measurements and interpretations
ANL/NDM-149, July 2000

A. B. Smith and A. Fessler
Neutrons and antimony:- neutronic evaluations of ^{121}Sb and ^{123}Sb
ANL/NDM-150, July 2000

A. B. Smith
Fast neutrons incident on Holmium
ANL/NDM-151, December 2000

R. D. Lawson and A. B. Smith
Technical note:- Dispersion contributions to neutron reactions
ANL/NDM-152, August 2001

A. B. Smith
Fast-neutrons incident on Hafnium
ANL/NDM-153, June 2001
D. L. Smith, Dimitri G. Naberejnev and L. A. Van Wormer
An approach for dealing with large errors
ANL/NDM-154, September 2001

ANL/NDM-155

FAST-NEUTRON SCATTERING FROM ELEMENTARY RHENIUM*

by

Alan B. Smith
Argonne National Laboratory, Argonne, Illinois; and
The Physicist's Consultative, Ottawa, Illinois

August 2003

Keywords:-
Measured neutron scattering, 0.3-1.5 MeV and 4.5-10 Mev. Optical-statistical and coupled-channels model analysis of experimental results. Basic and applied physical comments.

---

*This work supported by the United States Department of Energy under contract W-31-109-ENG-38.

TABLE OF CONTENTS

ANL/NDM-155

FAST-NEUTRON SCATTERING FROM ELEMENTAL RHENIUM

ABSTRACT

Results of measurements of neutron scattering from elemental rhenium are presented over two incident-energy regions:- 1) 0.3-1.5 MeV, and 2) 4.5-10.0 MeV. The first of these supplements previously-reported work at this Laboratory, and the second consists of information in an entirely new energy range. These experimental results are interpreted in terms of optical-statistical and coupled-channels models, including consideration of dispersive effects, and of scalar and vector potentials. Some basic and applied physical implications of these considerations are discussed. Comparisons are made with other regional and/or global models, and with evaluated nuclear-data files used in applications.

I. INTRODUCTION

Elemental rhenium consist of a pair of isotopes:- ^{185}Rh (37.4% abundant) and ^{187}Rh (62.6% abundant). Both are highly deformed collective rotors and the low-lying structure of each is built upon the $K=5/2^+$ band ($5/2^+$ [402]) with the particle configuration $(7/2^+)^2$ $(5/2^+)(9/2^-)^2$ arising from the $d^{5/2}$ shell [(MN59); (Pre62)]. Ground states are $5/2^+$ for both isotopes. The first excited states are $7/2^+$, and at approximately 130 keV, followed by $9/2^+$ levels at an excitation of approximately 300 keV. The next single-particle configuration is $(7/2^+)^2$ $(5/2^+)^2$ $(9/2^-)$ with a $K=7/2^-$ ($9/2^-$ [514]) rotational band. In ^{185}Re the head of the latter band is at an excitation of approximately 370 keV, and in ^{187}Re at approximately 210 keV. With these structure configurations one would expect relatively strong collective effects in fast-neutron elastic- and inelastic-scattering processes. The only thing that is experimentally known of fast-neutron scattering from rhenium is the result of work at this Laboratory; some very early work at lower energies (SGW68) and the present lower-energy and 4.5 - 10 MeV scattering results. There is no other rhenium experimental fast-neutron-scattering information. The experimental knowledge of rhenium neutron total cross sections is little better, as summarized in **Appendix A-1**. At low energies neutron capture information is available (MY87) but it has a minor effect upon fast-neutron scattering. This lack of experimental neutron-scattering information for the masses in this region of collective deformation is, unfortunately, quite typical.

Rhenium is well above the heavy fission-product region and thus not generally a concern in conventional fission-reactor fuel-cycle considerations. However, the metal is a high-temperature corrosion-resistant material for special uses; for example, in high-temperature nuclear space-power sources. Moreover, it is desirable to improve the systematics of the understanding of the neutron interaction with nuclei in this mass region as nearby targets are a matter of wide practical concern. It was for these purposes that the present work was undertaken.

II. EXPERIMENTAL PROCEDURES AND RESULTS

The neutron total cross sections associated with this work are outlined in **APPENDIX A-1**. One of the larger blocks of this data is the result of early work by this group (SGW68). Unfortunately, the experimental neutron total cross sections are not particulary consistent in the few-hundred keV to several MeV region, and do not extend above approximately 15 MeV.

Elastic- and inelastic-scattering cross sections at incident energies of less than 1.5 MeV were reported by the author's group some time ago (SGW68). Since that report, a number of additional differential elastic- and inelastic-scattering measurements have been made over the same lower-energy 0.3 - 1.5 MeV range. All of these measurements employed the time of flight technique ((CL55) with eight flight paths of about 2.5 meters length. Eight to ten measurements were distributed over the angular range of 25 - 160 degrees at each incident energy. The neutron source was the ^{7}Li(p,n)^{7}Be reaction (Dro87) below neutron energies of 1.5 MeV. This reaction emits a second neutron group that distorts inelastic-scattering results at excitations of approximately 450 - 500 keV. Appropriate corrections introduce additional uncertainties. Below incident energies of 1.5 MeV the scattered neutron resolutions were 25 - 50 keV, sufficient to resolve a great deal of the structure in the inelastic-scattering results. In total approximately 118 scattered-neutron elastic and inelastic distributions were measured at incident energies of less than 1.5 MeV, about half of which have been published in the earlier work. All of these lower-energy measurements were made relative to carbon or zirconium total neutron scattering as reported in ref. (Lan+61). The lower-energy elastic-scattering results were energy-averaged and collapsed into twelve distributions in order to smooth fluctuations and reduce the statistical uncertainties. The resulting averaged distributions are illustrated in the left panel of **Fig. II-1**. The corresponding lower-energy inelastic-scattering results are discussed in **Sec. III-C**, below.

The second portion of the neutron-scattering measurements covered the neutron energy range 4.5 - 10 MeV with twelve approximately equal-energy-spaced distributions. Each of these higher-energy measurements involved approximately forty differential values distributed between approximately 25 and 160 degrees. The ^{2}D(d,n)^{3}He reaction (Dro87) was used as a neutron source at incident energies above 4.0 MeV, with the deuterium contained in a gas cell. The scattered-neutron resolutions were approximately 200 - 300 keV. Therefore, the inelastic scattering resulting from the excitation of low-lying levels of the rhenium isotopes was not clearly resolved. These higher-energy measurements involved the concurrent use of ten flight paths, each approximately five meters in length. Cross sections were measured relative to the H(n,n) scattering standard (CSL83). The higher-energy "elastic"-scattering results are illustrated in the right panel of **Fig. II-1**.

All of the measurements used cylindrical samples of high-purity elemental metallic rhenium, approximately 2.0 cm in diameter and 2.0 cm long, placed 10 - 15 cm. from the neutron

source, at a zero-degree source-reaction angle. All of the experimental results were corrected for angular-resolution, beam attenuation and multiple-event effects using monte-carlo procedures (Smi90). These correction procedures were carried out in an iterative manner.

Various versions of the time-of-flight system used in the above measurements operated at The Argonne National Laboratory for over thirty years. They are well described elsewhere (Smi+92).

III. PHYSICAL MODELS

III-A. OPTICAL-STATISTICAL MODEL (SOM)

The weak-coupling optical-statistical model (SOM) [(Wol51); (Fes58)] was assumed as the starting point for the physical modeling. It is an energy-average model, reflecting gradual energy-dependent trends of the experimental observables, but not the detailed underlying resonance structure. Above a few keV the microscopic resonances underlying the observed phenomena grossly overlap to form smooth energy-dependent averages consistent with the SOM concepts, therefore the present considerations start at 50 keV and extend upward in energy to approximately 15 MeV. The model considerations were terminated at the latter energy due to the complete lack of experimental information at higher energies, but the models may extrapolate the observables to higher energies with some reliability. Throughout this work the real potential is assumed to have the Saxon-Woods form, the absorption (imaginary) potential the Saxon-Woods-Derivative form, and the spin-orbit potential the Thomas form (Hod63). Both direct and compound-nucleus interactions were given detailed attention. Eighteen ^{185}Re and eighteen ^{187}Re excited states were explicitly considered up to excitation energies of approximately 1.0 MeV. The respective excitation energies, spins and parities were taken from the Nuclear Data Sheets (**NNDC**). Higher-energy excitations were considered in the context of statistical evaporation processes as set-forth by Gilbert and Cameron (GC65). The calculations included resonance width-fluctuation and correlation corrections following the methods of Moldauer (Mol80). Compound-nucleus processes were considered only as relevant to neutron total and scattering processes. Multiple-neutron and charged-particle emission is not significant at the energies of the present work, and radiative capture is too small to make a significant effect over the region of interest here (MY87). All of the SOM calculations were carried out using the code ELEMENTAL ABAREX (Smi99), which, in this case, concurrently treats each of the two isotopes of elemental rhenium. In doing so real and imaginary iso-vector potentials can be examined, assuming the same geometries as those of the scalar potentials. The spin-orbit potentials were fixed to the real values of ref. (WG86). An additional small imaginary spin-orbit potential was not considered, and there is debate in the literatures as to whether it exists. Consideration of alternate spin-orbit potential choices (not discussed here) had very little effect on the results.

The real and imaginary spherical optical-statistical model (SOM) parameters were

determined by explicitly least-square fitting the neutron total and differential scattering cross sections. Throughout this work, the model fitting proceeded through six sequential steps. I) Six parameter fitting varying real and imaginary potential parameters from which the real-potential diffuseness, a_v, was fixed and the fitting proceeded to the next step. II) Five parameter fits from which the real-potential reduced radius, r_v where $R_v = r_v A^{1/3}$, was determined and fixed for the subsequent steps. III) Four parameter fitting from which the reduced imaginary-potential radius, r_w, was determined and fixed. IV) Three parameter fits from which the imaginary diffuseness, a_w, was determined and fixed. V) Two parameter fitting giving the real, V, potential strengths. And finally, step VI) from which the imaginary potential, W, was determined. The entire procedure was repeated several times in an iterative manner, using the results of the prior fitting cycle as the starting point for the current one. The data base for the fitting included all of the differential-scattering data of **Fig. II-1**. The uncertainties of the scattering data were taken as indicated by the measurements except for the low-energy averaged data where 5% was subjectively chosen. The total cross sections at the energies of the scattering measurements were concurrently included in the fitting procedures.. In doing so the available experimental total-cross-section values were averaged over approximately 100 keV and given a weight that was equivalent to that of four or five differential-scattering values. As noted above, the experimental resolutions used in the scattering measurements below approximately 1.5 MeV were such as to resolve the elastic from all inelastic-scattering components. However, for the higher-energy set (4.5 - 10 MeV) the observed scattering distributions included the contributions due to the excitation of the first two or three excited levels of each isotope with the elastic component. The fitting was adjusted so as to include the inelastic contributions with the elastic scattering to reflect the experimental resolution effects above 4.0 MeV.

The above fitting procedures led to the SOM parameters given in **Table III-A-1** (Throughout this work potential parameters are given to sufficient precision to make possible accurate reproduction of calculated results. These precisions do not imply uncertainties.) These parameters have their peculiarities which may reflect the inappropriateness of the simple SOM for describing the fast-neutron interaction with these two highly collective rotational isotopes. There are several causes for concern. The real-potential strength is essentially constant with energy, not decreasing with energy as one would expect from the non-locality of the nuclear force (PB62), and as encountered in commonly used "global" and "regional" models [(KD03), (Hod94)]. The real reduced radius is unusually small. This tends to be characteristic of SOM representations of the neutron interaction with highly collective targets in this mass region [(Smi01); (Smi02)]. The imaginary-potential strength has two branches reflecting a sharp energy dependence. The imaginary reduced radius is unusually large, and the imaginary diffuseness is quite small at low energies and rapidly increases with energy. This SOM parameter set is based upon the interpretation of the present experimental work which extends only to ten MeV. Extrapolation to higher energy, as discussed below in the context of dispersion effects, may be valid to some extent. Despite these difficulties, the SOM of **Table III-A-1** may be of practical use in some applications. It does give a very good representation of the neutron total cross section of elemental rhenium from a few keV to more than 15 MeV, as illustrated in **Fig. III-A-1**. The calculated results are within several percent of the measured values. Deviations between

measurement and calculation are less than variations between the experimental sets alone. Furthermore, the experimental-total-cross-section sets are not entirely consistent in magnitude and energy-dependent shape which, and the latter not entirely consistent with any optical-model shape.

The SOM does not do as well describing the measured "elastic" scattering distributions, as illustrated in **Fig. III-A-2.** The agreement between measurement and calculation is reasonably good up to incident energies of approximately 1.5 MeV. In this low-energy region the compound-elastic contribution is strongly effected by competition with compound-nucleus inelastic processes which were given detailed attention in the calculations. Above approximately 1.0 - 1.5 MeV the measured "elastic" distributions also probably include growing contributions from inelastic scattering which increasingly is dominated by direct-reaction processes involving the collective rotational properties of the two rhenium isotopes. Such direct-reaction processes are beyond the scope of the SOM and are dealt with below in the context of rotational coupled-channels models. The consequence is a distortion of the SOM scattering calculations in the few-MeV region, particularly in the minima of the measured distributions which contain significant inelastic direct-reaction contributions . As the incident energy further increases the simple SOM tends to better describe the observations. However, there remains distortion due to te neglect of direct processes.

III-B. SPHERICAL SCALAR AND VECTOR POTENTIALS (SOMV)

From basic concepts of nuclear forces and supported by some experimental evidence [(GPT68); (Sat69); (Hod94) and(BG69)] the real and imaginary SOM potentials are believed to take the forms

$$V = V_0 \mp V_1 \cdot \eta$$

and **(III-B-1)**

$$W = W_0 \mp W_1 \cdot \eta,$$

where V_0 (W_0) is the "scalar" term and V_1 (W_1) is the "vector" term, η is the nuclear asymmetry equal to (N-Z)/A, and the signs are negative for neutron induced processes and positive for proton processes. Various values of V_1 are found in the literature, generally in the range 15 - 30 MeV, with 16 and 24 MeV commonly used values [(MY87) and (Smi00)]. The imaginary "vector" values are generally taken to be half those of the real potential. The two isotopes of rhenium were dealt with in detail in the above SOM derivation, including size, compound-nucleus structure and natural abundance. However, the asymmetry and its implications on the potential were not considered. The asymmetries of ^{185}Re and ^{187}Re differ by less than 4%. Therefore, the impact of the "vector" term of **Eq. III-B-1** is small; e.g., for a typical V_1 value of 16 MeV the real potentials of the two isotopes will differ by approximately 0.7 MeV, a value which is less than 1.5% of the entire real potential and thus hard to detect from experimental interpretations. The impact of W_1 is even smaller.

Despite the above considerations that suggest that the impact of the scalar-vector form of the potential will be very small in the current context, the matter was investigated and termed the spherical-optical-model-vector potential (SOMV). In the first attempt the geometries of the simple SOM (**Table III-A-1**) were assumed and the strength of V and W determined by fitting, as described in **Sec. III-A**. V_1 was set equal to 16 MeV and W_1 equal to 8 MeV, as used in ref. (MY87). This two-parameter fitting procedure resulted in V_0 = 48.996 + 0.08589·E and W_0 = 16.553 - 2.0175·E (for E less than 5.62 MeV), and W_0 = 3.4719 + 0.35674·E (for E above 5.62 MeV). It should be emphasized that i) the asymmetry is fixed by the target A and Z, ii) that these are neutron interactions thus the signs of **Eq. III-B-1** are negative, and iii) that the vector strengths are fixed by assumption (e.g., V_1 = 16 MeV in this example). Thus the fitting procedure yields the scalar potentials V_0 and W_0. These must be corrected in an obvious way for direct comparison with the V and W values of **Table III-A-1.** When this is done the agreement with the values of **Table III-A-1** is remarkably good. For example, the zero-energy V values differ by approximately 0.2%. There are some differences in energy dependencies of the potentials, probably reflecting some small geometric changes between the SOM and SOMV concepts. Furthermore, it is reasonable to expect some geometric changes as the result of the introduction of **Eq. III-B-1**.

The full SOM fitting of **Sec. III-A** was extended to include the vector potentials of **Eq. III-B-1.** All the fitting procedures used to determine the SOM were explicitly repeated to obtain the SOMV, including selection of geometric factors. Two choices of V_1/W_1 were used; 16/8 MeV and 24/12 MeV). The resulting potential parameters are given in **Tables III-B-1** and **III-B-2**, respectively. The **Table III-B-1** SOMV potential gives a description of the observed rhenium total cross sections very similar to that obtained with the SOM over the energy range of the present interpretations, as illustrated by comparing **Fig. III-B-1** and **Fig. III-A-1.** Above 10 MeV the SOMV calculations tend to be several percent smaller than the results of the SOM calculations, and smaller than the measured values. This is the region of energy extrapolation of both the SOM and SOMV potentials as described in **Sec. III-C**. The discrepancy vanishes with alternate choices for extrapolation in energy. **Fig. III-B-2** compares the measured differential "elastic" scattering results (symbols) with the those of the SOMV calculation using the potential of **Table III-B-1**. The results are essentially identical to those obtained with the SOM and illustrated in **Fig. III-A-2**. The general character of the latter figure is similar to that of **Fig. III-A-2,** with some detailed differences in the minima of the distributions in the few-MeV region. Generally, the SOMV potential of **Table III-B-1** does not improve the description of the measured values over that of the SOM. Indeed, it may be somewhat inferior, but the differences are small and may be statistical artifacts from the fitting procedures. The "vector" potential of the above SOMV potential was increased to V_1/W_1 equal 24/12 MeV in order to examine the effect of alternate "vector" potential choices. 24 and 12 MeV are commonly used values found in the literature (Smi99A). The entire fitting procedure of the SOMV was again repeated resulting in the potential parameters of **Table III-B-2.** The calculated and measured total cross sections and differential "elastic" scattering cross sections were compared with results that were essentially identical to those illustrated in **Fig III-B-1** and **Fig. III-B-2**. Generally, it was

concluded that the various SOMV potentials lead to no improvement over the simple SOM potential in the present application. Any differences between results probably reflect reasonable statistical fluctuations in the respective fitting procedures. This is not surprising. As pointed out above, in this particular case of the two rhenium isotopes, the vector potential effects are very small, generally below the experimental sensitivity.

III-C. COUPLED-CHANNELS ROTATIONAL MODELS (ROTM)

Versions of the simple SOM may have their qualitative usefulness when applied to considerations of neutrons incident on rhenium. However, they fall qualitatively short of describing the scattering of fast neutrons from these two highly collective rotational isotopes. In particular, they do not describe the elastic or inelastic scattering by large amounts. One should expect the scattering between the $5/2^+$ (g,s.), $7/2^+$ ($E_x \approx$ 130 keV), and $9/2^+$ ($E_x \approx$ 300 keV) levels of the ground-state $K=5/2^+$ band to be strongly coupled. In the present interpretation these first three yrast states of the $5/2^+$ g.s. rotational band of each of the two isotopes were coupled together. The ^{185}Re deformations were initially taken to be $\beta_2 = 0.22$ and $\beta_4 = -0.085$ and those of ^{187}Re to be $\beta_2 = 0.21$ and $\beta_4 = -0.085$ as indicated by systematics and cited in the literature [(GPA72) and ((MY87)]. With these choices a comprehensive rotational fitting procedure was carried out using the geometric form factors of the above SOM and a similar fitting rational. All of the calculations employed the coupled-channels method (Tam65) implemented with the coupled channel code ECIS (Ray96). The latest version of that code will handle compound-nucleus processes in the same way as the **ABAREX** used in the SOM fit. However, total cross sections were not included in the ROTM fitting. Each step of the fitting consisted of a ^{185}Re and a ^{187}Re calculation assuming that the experimental data applied only to that isotope. The resulting two parameters sought in that particular step of the fitting were then averaged, weighting with the isotopic abundance, to obtain the "elemental" value. The procedure clearly does not consider vector potential effects but those have been shown to be negledgable in the present application (see above SOMV considerations). All the fitting was done with the differential scattering measurements. The total cross sections were considered only in comparisons with the calculated results after the fitting. This is a slow procedure but it gives good results.

The simple ROTM elemental parameters following from the above fitting procedure are given in **Table III-C-1.** These parameters lead to the elemental neutron total cross sections compared with the available experimental information in **Fig. III-C-1.** The quality of the description of the experimental results approaches that of the SOM even though no total cross sections were involved in the fitting, as in the SOM case. This suggests that the measured total and differential-scattering cross sections are reasonably consistent. **Fig. III-C-2** compares the experimental scattering data base with the results of calculations using the ROTM of **Table III-C-1.** The experimental observables are well described by the model. In particular, the large discrepancies so evident with variants of the SOM are not present. This is clearly a reflection of the rotational nature of the model in this application. The calculations also support the

experimental resolutions used in fitting the data. Below incident energies of 1.5 MeV the single elastic distributions are reasonably consistent with the measured values as one would expect from the estimated experimental energy resolution. Above approximately 4.0 MeV the calculations combining the elastic contribution with those from the first two inelastic groups of the g.s. rotational band are clearly most consistent with the data, as expected from the estimated energy resolution of the measurements.

The above elemental ROTM results are quite consistent with those obtained if one treats ^{185}Re and ^{187}Re individually and assumes that the experimental elemental data is explicitly applicable to either of the isotopes. With these assumptions the above isotopic fitting procedures were repeated individually for each of the two isotopes to obtain "isotopic" potential parameter sets. These are given illustrated by the ^{187}Re example of **Table III-C-2**, and corresponding comparisons between measured and calculated results given in **Figs. III-C-3** and **4**. Clearly, the isotopic potential parameters and the comparisons with the measured values are very similar to those obtained for the elemental model. This again suggests that "vector" potential effects are not a serious consideration in the present application, and that the differences due to compound-nucleus properties and size effects are small.

The present inelastic-scattering results were combined with the early work of ref. (SGW68). The combined sets were ordered by incident and excitation energy, and then averaged over approximately 50 keV incident-energy bins. Uncertainties were assigned to the averaged values as estimated by the author. These inelastic-scattering excitation functions are correlated with the known excited levels in the isotopes of ^{185}Re and ^{187}Re in **Table III-C-3.** At the lower excitation energies these correlations between reported isotopic structure and observed inelastic-scattering are quite straightforward. However, as the excitation energy increases the correlation between reported excitations and observed inelastic scattering becomes increasingly uncertain. The first four inelastically-scattered neutron groups seem quite clearly associated with well-defined levels in the two rhenium isotopes. The fifth observed inelastic-neutron group is in the energy region which is distorted by the second neutron group of the source reaction, as noted above. It doubtless consists of contributions from three reported levels in the two isotopes, but also includes large contributions from elastic-scattering of the second source-reaction group. This conclusion is strongly supported by the cross section magnitudes, as discussed below. The sixth, and final, inelastic group of **Table III-C-3** may be associated with at least six reported levels in the two isotopes. At least four additional inelastic-neutron "groups" were observed but, in the context of the rapidly increasing level densities of each of the two isotopes and deteriorating experimental energy resolution, correlation between observation and level structure rapidly deteriorates above excitations of 0.6-0.7 keV, and no attempt was made to establish such associations. The cross sections for the above excitations were calculated with the ROTM potential with the results shown in **Fig. III-C-5.** For the first excited level (1) the calculated results are significantly larger than the measured values. The agreement between measured and calculated results for levels 2, 3, 4 and 6 is reasonably good given the uncertainties in the measured and calculated values. The measurements relative to level 5 are grossly larger than predicted by the model. This is the level greatly distorted by the elastic scattering of the second

group from the source reaction, as noted above. The calculation of the excitation of the first (1) level is a concern. The calculated values are significantly larger than the measured quantities over much of the experimental energy range. There can be little doubt that the observed cross sections are due to excitation of the first (7/2+) levels in each of the rhenium isotopes. Furthermore much of the cross section consists of the direct-reaction component which is strongly influenced by the magnitude of β_2, The comparisons of **Fig. III-C-5** suggest that the β_2 used in the above ROTM calculations is too large. The entire ROTM fitting, outlined above, was repeated with smaller values of β_2. After several attempts it was concluded that the inelastic excitation of the first level was best calculated when the β_2 of each isotope was reduced by approximately 15% from the values used in the above ROTM calculation. The potential parameters following from the fitting with these small values are summarized in **Table III-C-4.** The resulting calculated inelastic excitation of the first level was in much improved agreement with experiment, as illustrated in **Fig. III-C-6**, and the description of the differential-scattering distributions was essential the same as achieved with the ROTM potential, as illustrated in **Fig. III-C-7**. The evidence is not unequivocal, but the inelastic-scattering measurements suggest that the β_2 initially used in the ROTM model, and as reported in the literature is too large. More precise scattering evidence may well support this conclusion.

III-D. DISPERSION EFFECTS

It is well known that there is a dispersion relationship coupling real and imaginary potentials and reflecting causality [(Sat83); (Lip66); (Pas67) and (Fes58)]. This relationship is frequently expressed in the form

$$J(E)_V = J(E)_{HF} + (P/\pi)\cdot\int [\, J_w(E')/(E - E')]\cdot dE' \qquad \textbf{III-D-1}$$

where J_V is the strength of the real potential, J_{HF} that of the local-equivalent Hartree-Fock potential, and J_W the strength of the imaginary potential. "P" is the principle value of the integral which is evaluated from $-\infty$ to $+\infty$. Here, and throughout this discussion, strengths are give in the form of volume-integrals-per-nucleon unless otherwise stated. The above integral can be broken into surface, ΔJ_{sur}, and volume, ΔJ_{vol} components

$$\Delta J_{sur} = (P/\pi)\cdot\int [J_{sur}(E')/(E - E')]\cdot dE' \qquad \textbf{III-D-2}$$

and

$$\Delta J_{vol} = (P/\pi)\cdot\int [J_{vol}(E')/(E - E')]\cdot dE'. \qquad \textbf{III-D-3}$$

Then $J_{vol}(E) = J_{eff}(E) + \Delta J_{sur}(E)$ and $J_{eff}(E) = J_{HF}(E) + \Delta J_{vol}(E)$, where $J_{sur}(E)$ and $J_{vol}(E)$ are surface- and volume-imaginary potential strengths, respectively. J_{HF} and ΔJ_{vol} are both approximately linear functions of energy in the range of the present considerations thus individual components can not be experimentally resolved in the present work. The effect of

Eq. III-D-2 is to add a surface component to the real potential that is some portion of the imaginary potential. The magnitude of this contribution can be calculated using the methods of Lawson (LGS87) and Lawson and Smith (LS01). The latter reference presents a detailed description of the theory and method and includes a FORTRAN source code for executing the calculations. In the present application it was assumed that ΔJ_{sur} retained the geometric parameters and Saxon-Woods-Derivative form of the imaginary potential, varying only in magnitude. This is an assumption that is not necessarily true, but there appears to be no guidance as to alternate shapes. The experimental data base and associated models are relevant to only a limited energy range of 10 MeV or less. It was assumed that the surface-imaginary potential was entirely a surface effect up to 10 MeV, and then fell linearly to zero at 80 MeV (this energy extrapolation was used in the above considerations). Concurrently, the volume-imaginary potential was taken to rise from zero at 10 MeV to 80 MeV where it took the J_{sur} 10 MeV magnitude, and then remained constant to infinity. Further, the imaginary potential was assumed to be zero at the Fermi Energy (E_F) and to have a quadratic energy dependence to zero energy. The Fermi energy was taken to be -7.0 MeV as determined from the mass tables (TUL90). Throughout, the considerations, the entire imaginary potential was taken to be symmetric about the Fermi energy.

Following the above outlined procedures and the methods of ref. (LS01), the above ΔJ_{sur} value was calculated from the simple spherical optical potential (SOM, **Table III-A-1**). These calculations assumed the higher-energy branch of J_w of **Table III-A-1** as being more representative of the SOM and less distorted by deformation effects. The calculations thus provide the contribution of the imaginary potential that must be reflected into the real potential due to dispersive effects. The energy dependence of the fraction of J_w that is reflected into the real potential is illustrated in **Fig. III-D-1.** It decreases from nearly unity at zero energy to modest negative values at 20 MeV. These magnitudes and energy dependancies are somewhat dependent on the energy extrapolations cited above. This dispersive fraction was converted to a potential fraction assuming the potential geometries of the SOM potential (**Table A-III-1**). As noted above, this assumption may not be entirely valid but other choices are not known

Using the above "DISP" contribution the entire fitting of the SOM potential, described above, was repeated in an iterative manner. The resulting SOM parameters are given in **Table D-III-1.** They are similar to those of the simple SOM (**Table III-A-1**). There are some changes in the real-potential geometry, as one would expect from the introduction of a surface real potential, and the real-potential strength is noticeably reduced. The corresponding calculated elemental rhenium total cross sections are in good agreement with measured values below 10-12 MeV, as illustrated in **Fig. III-D-2**, but then fall a bit low, suggesting that the higher-energy portions of the potential employed in calculating the dispersive contribution of **Fig. III-D-1** is not quite correct. The dispersive calculations result in the differential distributions shown in **Fig. III-D-3.** They are essentially the same as obtained with the simple SOM, as shown in **Fig. III-A-2.** Thus, while the dispersive effects are doubtless a physical reality, their application does not particularly improve the results of SOM experimental interpretations in the present rhenium context.

The above SOM dispersive exercise was repeated using the rotational (ROTM) model and resulted in the potential parameters of **Table III-D-2.** These values are consistent with those of the simple ROTM model given in **Table III-C-1.** They result in a reasonable description of the elemental rhenium total cross sections, as illustrated in **Fig. III-D-4.** The same is true for the calculated differential "elastic" scattering from elemental rhenium as illustrated in **Fig. III-D-5.** Again, though dispersive effects may well be a physical reality, they do not have significant effects in the present studies.

IV. BASIC AND APPLIED COMMENTS

The real radius of the above SOM is small as observed in spherical models of the neutron interaction with the neighboring rotational elements Ho and Hf [(Smi00) and (Smi01)]. There seems to be mounting evidence that this is characteristic of attempts to describe the neutron interaction with highly deformed rotational nuclei with an inappropriate SOM. Concurrently, unusual SOM energy-dependent imaginary-potential strengths and sizes are often encountered, as in this rhenium case. This simply is a reflection of the inappropriateness of the SOM in such applications. The rhenium ROTM real-potential geometries are similar to those of elemental Ho and Hf [(Smi00); (Smi00) and (Smi01A)], to those reported for relevant regional models (You86) and to systematics. For example, the systematics of ref.(Smi98) predict a Re a_v within 7% of that of the ROTM, and an r_v within 0.8% that of the ROTM. The r_V of ref. (You86) differ from those of the ROTM by only 1.2%, and the a_V by only 4.2%. The present ROTM r_w is 2.6% larger than that of Ho and Hf, and the a_w 8.8% smaller. However, in these cases the imaginary parameters are not as well defined so one should expect larger differences. Generally, the geometries of the present ROTM seem consistent with comparable rotational models in this mass region.

The above experimental interpretations are limited to 10 MeV and less. At these energies it was assumed that the absorption was entirely a surface phenomena. This is generally consistent with regional and global trends, as illustrated in ref. (MY87) where the onset of volume absorption is set at 9 MeV. The dispersion considerations, discussed above, introduce a volume absorption at 10 MeV, slowly increasing with energy. It is used in the extrapolations of the potentials to much higher energies and may not be quantitatively valid. A more serious concern at higher energies is probably the opening of additional neutron channels not considered in the present interpretations. In fact, neither the shapes or magnitudes of surface and volume absorptions are reasonably established at higher energies. Intuitively, one might expect that absorption slowly makes a transition from a surface property to a volume effect with increasing energy, rather than attributing absorption to two independent contributions.

The isotopic-spin dependence of the optical model results in proton and neutron potential strengths are related through the expression

$$J_i = J_{oi}(1 \mp \xi_i \cdot \eta) \qquad \textbf{(IV-1)}$$

where J_i are potential strengths expressed as volume-integrals-per-nucleon, η is the nuclear asymmetry (N-Z)/A, "i" may be either V or W for the real or imaginary potentials respectively, the sign is "+" for proton processes and "-" for neutron processes, and ξ_i is a constant (Lan62). Neutron scattering studies lead to ξ_V values near unity [(FCR77); (HW72) and (Smi98)]. However, these ξ_V values are nearly twice those suggested from nucleon-nucleon scattering and (p,n) studies. More accurately, **Eq. IV-1** should be (Chi+90)

$$J_V = (r_v)^3 \cdot K_{0V} (1 \mp \xi_V \cdot \eta) \qquad \textbf{IV-2}$$

where K_{0V} is a constant and r_v has an appropriate mass dependence (Chi+90). Using an r_v mass dependent expression such as ((Smi98)

$$r_v = 1.1685 + 0.37225/A^{1/3} \qquad \textbf{IV-3}$$

the neutron scattering data implies a ξ_V of approximately 0.5 , similar to the values suggested from nucleon-nucleon scattering and (p,n) studies [(Chi+90); (GMP70); ((GPT68) and (BFG69)]. However, **Eq. IV-1** is a reasonable starting point for comparing real-potential strengths over a limited mass range, but the results may be seriously influenced by shell and collective structural effects. In particular, coupling effects in interactions with highly collective nuclei, as in the present work, may very much distort the behavior predicted by **Eq. IV-1** (Com78). Recent work by the author has dealt with the fast-neutron interaction with three similar collective rotational targets; elemental Ho (^{165}Ho) (Smi00), elemental Hf ((Smi01A), and elemental Rh (the present work). The average elemental nuclear asymmetries of these three targets were found to be very similar, respectively 0.186, 0.193 and 0.195. In each case the fast-neutron interaction was described in the context of a coupled-channels model coupling the first three states of the g.s. rotational band. The real potential strengths for the three targets are; for Ho $J_V = 444.39 - 3.558 \cdot E$, for Hf $J_V = 455.98 - 2.587 \cdot E$, and for Re $J_V = 429.56 - 2.966 \cdot E$. These are very similar values with an average at E = 0 of 443.3 with a deviation of approximately 1.7%. At 10 MeV, the upper energy of the respective interpretations, the average is 412.9 with a derivation of 2.1%. Of, course, if one constructs the J_{0i} of **Eq. IV-1** the result will be essentially a renormalisation of the three J_V values depending on the magnitude of ξ_V one assumes. Because of the similarities of the asymmetries and the J_V magnitudes, the measurements of the neutron interaction with these three targets do not support or refute **Eq. IV-1** in the context of the real potential. The magnitudes of the imaginary strengths deduced from the measurements of the neutron interaction with the same three targets are; for elemental Ho $J_V = 22.4 + 2.151 \cdot E$, for elemental Hf $J_V = 19.5 + 2.419 \cdot E$, and for elemental Re $J_V = 18.3 + 2.258 \cdot E$. Again, the three values are very similar, with a zero energy average of 20.0 $\mp$ 6%, though there is a trend for the value to decrease with asymmetry as indicated by **Eq. IV-1**. As for the J_V values, they are consistent with **Eq. IV-1** but provide little further definition. **Eq. IV-1** relates the strengths of potentials in neutron and proton scattering. Unfortunately, the author could find no (p,p) scattering or (p,n) reaction data relevant to this work in the literature, and neither could information specialists at the NNDC.

Dispersive effects doubtless are a factor in the neutron interaction with the isotopes of

rhenium. With some simplifying assumptions, they were included in the above spherical and rotational interpretations. Their presence did not notably improve the description of the observables. There were some changes in the potential parameters (e.g., compare **Tables III-C-1** and **III-D-2**), generally of a form that one would expect from the introduction of the dispersion effect (e.g., some decrease in r_v). However, from the applied point of view, there is little justification for the additional complexity of the dispersion calculations in this particular case.

Attention was given to vector potentials in both a spherical and deformed context. Any effect they might have had was very much masked by the unavoidable experimental uncertainties in the data being analyzed. This conclusion is not surprising in view of the very similar asymmetries of the two isotopes of rhenium.

The above rotational potentials have energy dependencies that define the effective mass, m^*, through the equation

$$(m^*/m) = 1 - (dV^L/dE) \qquad \textbf{IV-3}$$

where m is the nucleon mass and V^L the local real potential. This ratio is 0.667 for the above ROTM rotational potential given in **Table III-C-1**. It is shown in refs. [(BDS79); (MN81) and (Bau+82)] that nonlocality leads to the expression

$$(m^*/m) = 0.64 + 0.36[1.0 + abs(E - E_F)/(2\hbar W_0)]^2 \qquad \textbf{IV-4}$$

where E_F is the Fermi energy and $\hbar W_0 = 41/A^{1/3}$. Well away from E_F **Eq. IV-4** leads to a (m^*/m) ratio of approximately 0.68 which is reasonably consistent with the nuclear matter estimate (GPT68) and remarkably close to the value indicated by the present ROTM potential. Concurrently, the zero end point of ROTM real potential is 148 MeV which approaches the global analysis of ref. (Bau+82). The above m^* considerations apply to the other variants of the rotational coupled-channels model discussed in **Sec. III** above. Clearly, the energy dependencies of the various SOM formulations are inconsistent with the above concepts.

The above discussion of inelastic scattering (**Sec. III-C**) and **Figs. III-C-5** and **III-C-6** suggests that the β_2 values for the two isotopes used in the primary ROTM rotational calculations are 10-20% too large. Alternatively, more complex coupling schemes may be more appropriate as in ref. (Com79). Unfortunately, the measured neutron inelastic-scattering data is not of sufficient quality or detail for a more quantitative examination of the degree of deformation. What is needed is a careful set of measurements of the cross sections for the inelastic excitation of the first few excited levels of both rhenium isotopes. Such measurements are feasible but difficult.

V. SOME COMPARISONS WITH OTHER MODELS AND WITH EVALUATIONS

V-A. COMPARISONS WITH OTHER POTENTIALS

There are a number of collective vibrational or rotational models of the fast-neutron interaction with nuclei in this mass region reported in the literature. It is of interest to compare the corresponding potentials to that of the ROTM of the present work. In making these comparisons a rotational rhenium model with the deformations of the ROTM (see **Table III-C-1**) was assumed. The corresponding strengths and geometries were taken as reported by the various authors. Nuclear asymmetry was considered when given. These comparisons were confined to the total cross sections to incident energies of 20 MeV, and to differential "elastic" scattering at energies of 4 to 10 MeV. Lower-energy scattering was not considered as those distributions are "bland" and not particularly sensitive to choice of potential. Inelastic scattering was not considered as there remains the question of the magnitude of the deformations (see above discussion). These potential comparisons are intended to be illustrative and are confined to the following five potentials:-

A. The reference point was taken to be the present ROTM potential (**Table III-C-1**). This was derived from explicit interpretations of experimental total and scattering cross sections of elemental rhenium, as described above..

B. The potential for the neutron interaction with holmium by Smith (Smi00). This potential was primarily deduced from the study of neutron total and scattering cross sections at energies of less than 10 MeV.

C. The potential given by Macklin and Young (MY86) in a study of rhenium neutron capture. It was apparently drawn from models in the rhenium mass region, and emphasized incident energies of less than 10 MeV.

D. This potential results from the study of neutron total and scattering cross sections of elemental hafnium, primarily at energies of less than 10 MeV (Smi01A).

E. A general potential for the fast-neutron interaction with holmium by P. Young (You86). The parameters are generally based on regional systematics.

Of course, there are a number of other relevant models in the literature that are used with varying degrees of success, but the above are generally representative of the situation for comparison purposes.

The fast-neutron total cross sections of elemental rhenium, as calculated with the above potentials (A-E) are compared with the available experimental information in **Fig. V-A-1**, Panel "A" of the figure references the ROTM potential of the present work. The calculated results are arguably lower than the measured values by a percent or two in some energy regions. As discussed in **Sec. III**, there are some questions about these small differences and the general energy dependence of the experimental values from which it is not clear that these small

differences do not reflect experimental problems within the limited data base. Panel B of the figure references potential B, above. That potential is largely based upon an interpretation of neutron scattering from holmium over the energy range 4-10 MeV. Over that energy range it gives a very good description of the rhenium total cross sections. The calculated total cross section results are not quite as suitable at lower and higher energies but the differences between calculated and measured values are relatively small (less than 5-6%). Panel C compares measured total cross sections with those calculated with the above potential C. The agreement is very good, perhaps arguably better than obtained with the reference ROTM. The calculated total cross sections tend to be slightly larger than the measured values over most of the energy range. Panel D compares measured values with those calculated with potential D. The later resulted from an interpretation of total and scattering cross sections of elemental hafnium, largely below 10 MeV. In the region of the primary scattering cross sections (4-10 MeV) the agreement is reasonably good, but at lower energies the calculations deviate from the measured rhenium values by large amounts. This reflects the physical reality that the measured hafnium and rhenium total cross section are very different. Panel E compares measured total cross sections with those calculated with potential E. Potential E is a regional representation and thus is not as specifically suitable as either the reference potential A or the specific rhenium potential C. These total-cross-section comparisons suggest, not surprisingly, that specific potentials based upon the rigorous interpretation of measured values are most suitable for total-cross-section prediction. Also, there are structural differences between nearby targets that can have a considerable effect on the corresponding potentials and their prediction of total cross sections (e.g., differences in rhenium and hafnium total cross sections at lower energies). Unfortunately, in the case of rhenium, experimental knowledge of neutron total cross sections is meager, and nonexistent above 15 MeV. Given the present experimental situation, the reference potential A (ROTM) or potential C give the best representations of rhenium total cross sections of the five potentials considered here.

The same type of comparisons are made between measured and calculated "elastic" scattering in **Fig, V-A-2**. The experimental reference is the 4.5-10 MeV scattering data of the present work. There is no higher-energy experimental information and the lower-energy measured values lack the "character" for reasonable comparisons. The same A through E potentials cited above are used, with "A" (the present ROTM) taken as the reference potential. It is evident from panel A of **Fig. V-A-2** that ROTM potential of the present work gives an excellent description of the measured values as discussed in **Sec. III-C**. The calculated distributions combining elastic and first two inelastic groups are in nearly exact agreement with measured values which have a corresponding experimental resolution. The agreement for potential B, as shown in panel B of the figure, is also good. This is perhaps not surprising as potential B was largely deduced from deferential scattering measurements in this energy range. As noted above, potential C does well in describing the total cross sections but it is not particularly good in describing the differential scattering as illustrated in panel C of the figure. Potential D is an improvement as illustrated in panel D. Like potentials A and B, its derivation was very much dependent on differential scattering in the 4.5 to 10 MeV region. The total-cross-section problems at lower energies do not persist into the scattering distributions at the energies

of **Fig. V-A-2**. Finally, the general E potential provides scattering distributions (panel E of the figure) that are not as consistent with experimental observations as are those from potentials A or B. The latter was explicitly derived from holmium scattering data while potential E has a more generalized background.

Comparisons of measured and calculated (ROTM potential) inelastic neutron-scattering excitation functions were discussed in **Sec. III-C** and illustrated in **Fig. III-C-4**. That discussion points out that the evident over-prediction of inelastic-scattering excitation functions suggests that the β_2 deformations used in the above comparisons are perhaps 15% too large. Therefore it is not productive to test potentials in the context of inelastic scattering until the deformations are better known.

The above comparisons of measurements and calculations suggest that several general regional potentials will give reasonable calculational results. However, potentials developed for neighboring nuclei are not always suitable for quantitative results. One should be cautious when using regional or generalized potentials in this mass region. When highly quantitative results are sought there is no substitute for a solid experimental basis for the development of models for interpolation and extrapolation. In the case of rhenium, such a data base is very meager.

V-B. COMPARISONS WITH SOME EVALUATED FILES

There are a number of evaluated neutronic file systems for applications studies distributed around the world. Most of them are devoid of either elemental or isotopic rhenium evaluations, or utilize older versions of the ENDF/B files. This may reflect low world-wide interest in neutronic systems containing rhenium. The ENDF/B-VI system does have recently upgraded ^{185}Re and ^{187}Re isotopic evaluated neutronic files. These can be compared with relevant portions of the present work.

Elemental neutron total cross sections constructed from the ENDF/B isotopic files are in very close agreement with what is experimentally known as illustrated in **Fig. V-B-1.** The differences between measured and evaluated results is no more than several percent and then largely in regions where the experimental values (particularly their energy dependencies) are suspect as noted elsewhere herein. These evaluated and measured results are in very close (essentially exact) agreement with the above ROTM model as shown. Minor differences between the model and the evaluation become evident only at energies approximately twice those of the present studies.

The present elastic-scattering results are compared with the isotopic values of END/B-VI in **Fig. V-B-2.** Over the energies of the present studies (below 10 MeV) the agreement between the present ROTM results and the isotopic values of END/B-VI is within a few percent, or within the experimental uncertainties alone. Above approximately 14 MeV the isotopic extrapolation of

the ROTM results in "elastic" cross sections that are increasingly larger than the evaluated quanities. As pointed out above, the present work is stickily valid only at energies of less than 10 MeV, and the considerations assume only neutron total and scattering cross sections are significant. Well above 10 MeV, the latter assumption breaks down as at approximately 15 MeV the (n,2n) cross section alone exceeds several barns. Thus it is mot surprising that the evaluated elastic-scattering cross sections are smaller than those predicted by the present models well above 10 MeV.

Comparisons of measured, calculated and evaluated inelastic-scattering cross sections are difficult due to the uncertain experimental cross sections and resolutions. However, END/B-VI reasonably represents the inelastic-scattering cross sections of the first few excited states as illustrated in **Fig. V-B-2**. Here the evaluated excitation of the inelastic excitation of the first excited state reasonably describes the present experimental summary. This a bit surprising as most of the models use deformations that tend to over-predict the excitation of the first level of the g.s. rotational band, as illustrated in **Fig. III-C-4**. The rational underlying the END/B-VI evaluation is not known to the author. However, this particular inelastic-scattering cross section was already reasonably defined by the early experimental work of ref. (SGW) at the time of the evaluation.

Possibly, in time, some improvement of rhenium evaluations can be achieved through better modeling and better understanding neutron-reaction systematics in the rhenium mass region. However, major improvements are probably going to require some comprehensive measurements.

VI. CONCLUDING REMARK

There should be no misunderstanding, the experimental knowledge of the fast-neutron interaction with rhenium, and neighboring nuclei, is in very sorry shape. Even the total cross sections of rhenium are very poorly known. Some of the desired measurements are difficult, but many of them involve the application of well-known techniques. The problem is that the facilities and professional skills to provide the requisite information are vanishing, and even the limited knowledge available is fading into the mists of time. With this lack of experimental information recourse is made to regional or global calculational models to provide information for applications. However, particularly in this deformed mass region, the calculational results are very sensitive nuclear structure effects. The models are most effective when they are used for interpolating between measured values.

As in a number of other cases, the experimental knowledge of (p,n) and (p,p) processes is largely nonexistent. This makes it difficult or impossible to assess some of the fundamental physical properties, particularly those dealing with iso-spin.

ACKNOWLEDGMENTS

The author would like to thank Drs. J. Raynal, P. Young and F. Kondev for their technical advice. The author is also indebted to the National Nuclear Data Center, Brookhaven Natl. Lab. for the efficient provision of essential nuclear data, and to Mr. J. Balling and associates for providing the computation facilities used in much of this work.

REFERENCES

(Bau+82) M. Bauer et al., J. Phys. **G8** 525 (1982).

(BFG69) C. Batty, E. Friedman and G. Greenlees, Nucl. Phys. **A127** 368 (1969).

(BG69) F. Becchetti Jr., and G. Greenlees, Phys. Rev. **182** 1190 (1969).

(BDS79) G. Brown, J. Dehesa and J. Speth, Nucl. Phys. **A330** 290 (1979).

(Chi+90) S. Chiba, P. Guenther, R. Lawson and A. Smith Phys. Rev. **C42** 2487 (1990).

(CL55) L. Cranberg and J. Levin, **Proc. Conf. on Peaceful Uses of Atomic Energy** Geneva, United Nations Press (1958).

(Com79) J. Comfort, Phys. Rev. Lett. **42** 30 (1979)

(CSL83) Editors:- H. Conde, A. Smith and A. Lorenz, Nuclear Standards File, **IAEA Tech. Report 227** (1983).

(Dro87) M. Drosg, IAEA Report **IAEA-TECDOC-410** (1987).

(END/B) Evaluated Nuclear Data File-B-VI, National Nuclear Data Center, Brookhaven Natl. Lab.

(FCR72) J. Ferrer, J. Carlson and J. Rapaport, Nucl. Phys. **A275** 325 (1977).

(Fes58) H. Feshbach, Ann. Rev. Nucl. Sci. **8** 49 (1958).

(GC65) A. Gilbert and A. Cameron, Can. J. Phys. **43** 1446 (1965).

(GMP70) G. Greenlees, W. Makofske and G. Pyle, Phys. Rev. **C1** 1145 (1970).

(GPA72) U. Goetz, H. Pauli and K. Adler, Nucl. Phys. **A192** 1 (1972).

(GPT68) W. Greenlees, G. Pyle and Y. Tang, Phys. Rev. **171** 1115 (1968); also Phys Rev. **C1** 1145 (1970).

(Hod63) P. Hodgson, **The Optical Model of Elastic Scattering** Clarendon, Oxford (1963).

(Hod94) P. Hodgson, **The Nucleon Optical Model** World Sci. Pub., Singapore (1994)

(HW72) B. Holmqvist and T. Wiedling, Nucl. Phys. **A188** 24 (1972).

(KD03) A. Koning and J. Delaroche, Nucl. Phys. **A713** 231 (2003)

(Lan+61) R. Lane et al., Ann. Phys. **12** 135 (1961).

(Lan62) A. Lane, Nucl. Phys. **35** 676 (1962); also Phys. Rev. Lett. **8** 171 (1962).

(LGS87) R. Lawson, P. Guenther and A. Smith, Phys. Rev. **C36** 1298 (1987).

(Lip66) R. Lipperheide, Nucl. Phys. **89** 97 (1966).

(LS01) R. Lawson and A. Smith, Argonne Natl. Lab. Report **ANL/NDM-152** (2001).

(MN59) B. Mottelson and S. Nilsson, Kgl. Danske Videnskab Selskab. Mat. Fys. Skrifter **1** 8 (1959).

(MN81) C. Mahaux and H. Ngo, Phys. Lett. **100B** 285(1981).

(Mol80) P. Moldauer, Nucl. Phys. **A344** 185 (1980).

(MY87) R. Macklin and P. Young, Nucl. Sci. and Eng. **97** 239 (1987).
(NNDC) National Nuclear Data Center, Brookhaven Natl. Lab.
(Pas67) G. Passatore, Nucl. Phys. **A95** 694 (1967).
(PB62) F. Perey and B. Buck, Nucl. Phys. **32** 353 (1962).
(Pre62) M. Preston, **Physics of the Nucleus** Addison-Wesley, Reading, MA (1962).
(Ray96) J. Raynal, The Coupled Channels Code **ECIS96**, private communication, see also CEA Report **CEA-N-2772** (1994).
(Sat69) G. Satchler, **Iso-spin in Nuclear Physics**, ed. D. Wilkinson, North-Holland, Amsterdam (1969).
(Sat83) G. Satchler, **Direct Nuclear Reactions** Addison-Wesly, Reading, MA (1983).
(SGW68) A. Smith, P. Guenther and J. Whalen, Phys. Rev. **168** 1344 (1968).
(Smi90) A. Smith, **Argonne Momorandum** (1990), unpublished.
(Smi92) A. Smith, Argonne Natl. Lab. Report **ANL/NDM-127** (1992); see also Phys. Rev.**C45** 1260 (1992); Z. Phys. **A360** 265 (1982); Nucl. Instr. and Methods **50** 277 (1977); and references cited therein.
(Smi98) A. Smith, J. Phys. **G24** 637 (1998).
(Smi99) A. Smith, Argonne Natl. Lab. Report **ANL/NDM-147** (1999).
(Smi99A) A. Smith, Argonne Natl. Lab. Report **ANL/NDM-142** (1999).
(Smi00) A. Smith, Argonne Natl. Lab. Report **ANL/NDM-151** (2000).
(Smi01) A. Smith, Ann. Nucl. Energy **28** 1745 (2001).
(Smi01A) A. Smith, Argonne Natl. Lab. Report **ANL/NDM-153** (2001).
(Smi02) A. Smith, Ann. Nucl. Energy **29** 1241 (2002).
(Tam65) T. Tamura, Rev. Mod. Phys. **37** 679 (1965).
(Tul90) J. Tuli, **Nuclear Wallet Cards,** National Nuclear Data Center, Brookhaven Natl. Lab. (1990).
(WG86) R. Walter and P. Guse, **Proc. of Conf. on Nucl. Data for Basic and Applied Sci.** Eds. P. Young et al., **2** 272, Gordon and Breach, New York (1986).
(Wol51) L. Wolfenstein, Phys. Rev. **82** 690 (1951).
(You87) P. Young, Los Alamos Natl. Lab. Report **LA-10689-PR** (1987).

APPENDICES

A-1. PRIOR NEUTRON TOTAL-CROSS-SECTION DATA

There are only five references giving neutron total cross sections of rhenium or its isotopes that are relevant to the present considerations (as referenced below). These results are illustrated in **Fig. A-1**. Given the sparsity of experimental information, the experimental results are qualitatively fairly consistent within themselves and with the END/B-VI evaluation, as illustrated in **Fig. A-1**. However, it would be well to have several verification measurements below energies of approximately 15 MeV, and nothing seems to be known at higher energies. All of the relevant results from the literature are for elemental rhenium.

(SMS76) D. Stupegia, A. Madson and M. Schmidt, private communication, 1976 (*12125, asterisks denote EXFOR numbers). Many monoenergetic-source results extending from approximately 10 keV to 1.9 MeV. Resolutions 10-20 keV.

(TS68) R.Tabony and K. Seth, Ann. Phys.**46** 401, 1968 (*11953). Many monoenergetic results extending from approximately 30 to 650 keV. Resolution several keV.

(SGW68) A. Smith, P. Guenther and J. Whalen, Phys. Rev. **168** 1344,1968 (*10631). Many monoenergetic results extending from approximately 0.5 to 1.5 MeV. Resolution a few keV.

(DV72) W. Dilg and H. Vonach, EANDC(E)-**150** 40, 1972 (*20583). A single value at 3 keV.

(FG71) D. Foster and D. Glasgow, Phys. Rev. **C3** 576, 1971 (*10047). Detailed white-source results with many values distributed between approximately 2.2 and 14.9 MeV.

A-2. PRIOR NEUTRON ELASTIC-SCATTERING DATA

There appear to be only two measurements of neutron elastic scattering from rhenium or its isotopes (A. Smith, P. Guenther and J. Whalen, Phys. Rev. **168** 1344,1968 (*10631); and V. Nikolenko, A. Popov and G. Samosvat, INR-P3 **85** 133,1985 (*40937); again, numbers preceded by the asterisk are EXFOR reference numbers). The former gives comprehensive coverage from 0.3 to 1.5 MeV with a number of scattered-neutron angular distributions. The latter reference presents some low-energy pulsed-reactor data and only very fragmentary differential information at approximately 450 keV. Before the present results, knowledge of "elastic" neutron scattering from rhenium or its isotopes was essentially limited to the energy range 0.3 - 1.5 MeV and one set of measurements.

A-3. PRIOR NEUTRON INELASTIC-SCATTERING DATA

Prior measurement of neutron inelastic scattering from rhenium and/or its isotopes is limited to one reference ((SGW68) A. Smith, P. Guenther and J. Whalen, Phy. Rev. **168** 1344,1968; *10631). That work is more than 35 years old and confined to incident energies of less than 1.6 MeV. Interestingly, that early inelastic-scattering work suggested shortcomings in the contemporary knowledge of the excited structure of rhenium, particularly ^{185}Re. These deficiencies have been largely removed through later structure work, as summarized in the Nuclear Data Sheets. These early inelastic-scattering results were combined with the present results as discussed in **Sec. III-C**.

TABLES

Table III-A-1:- Parameters for the simple SOM potential. Particle energies (E) and potential strengths (V and W) are given in MeV and geometries in fermis. Approximate strengths in volume-integrals-per-nucleon (J) are in units of MeV-fm^3. These parameters are relative to incident energies of less than 10 -12 MeV. This is entirely an iso-scalar potential:- i.e., $V_1=W_1=0$ of **Eq. III-B-1**.

Real Potential

Strength

$V = 45.931 - 0.04937 \cdot E$

$J_V = 380.02 - 0.4085 \cdot E$

Reduced Radius

$r_v = 1.2196$

Diffuseness

$a_v = 0.6607$

Imaginary Potential

Strength

$W = 14.713 - 1.9038 \cdot E$, for E less than 5.62 MeV

$J_w \approx 79.18 - 8.73 \cdot E$

$W = 2.0750 + 0.34392 \cdot E$, for E greater than 5.62 MeV

$J_w \approx 11.17 + 3.91 \cdot E$

Reduced Radius

$r_w = 1.3384$

Diffuseness

$a_w = 0.3391 + 0.02293 \cdot E$

Spin-Orbit Potential (WG86)

Strength

$V_{so} = 6.157 - 0.015 \cdot E$

Reduced Radius

$r_{so} = 1.103$

Diffuseness

$a_{so} = 0.56$

Table III-B-1:- Parameters for the SOMV potential. Particle energies (E) and potential strengths (V and W) are given in MeV and geometries in fermis. Approximate strengths in volume-integrals-per-nucleon (J) are in units of MeV·fm^3. This is an iso-vector potential with V_I=16 MeV and W_I = 8 MeV. This potential is valid to 10-12 MeV.

Real Potential

Strength

$V = 49.930 + 0.20568 \cdot E$

$J_V = 385.78 + 1.5892 \cdot E$

Reduced Radius

$r_v = 1.1920$

Diffuseness

$a_v = 0.6467$

Imaginary Potential

Strength

$W = 14.245 - 1.5217 \cdot E$, for E less than 6.165 MeV

$J_W \approx 78.74 - 5.78 \cdot E$

$W = 3.6126 + 0.20257 \cdot E$, for E greater than 6.165 MeV

$J_W \approx 19.97 + 4.19 \cdot E$

Reduced Radius

$r_v = 1.3409$

Diffuseness

$a_w = 0.3469 + 0.03291 \cdot E$

Spin-Orbit Potential is as given in **Table III-A-1** (WG86).

Table III-B-2:- Parameters for the SOMV potential. Particle energies (E) and potential strengths (V and W) are given in MeV and geometries in fermis. Approximate strengths in volume-integrals-per-nucleon (J) are in units of MeV-fm^3. This is an iso-vector potential with $V_1 = 24$ MeV and $W_1 = 12$ MeV. The parameters are valid to 10-12 MeV.

Real Potential

Strength

$V = 51.729 + 0.23137 \cdot E$

$J_V = 392.59 + 1.7560 \cdot E$

Reduced Radius

$r_v = 1.1864$

Diffuseness

$a_v = 0.6286$

Imaginary Potential

Strength

$W = 16.796 - 1.8332 \cdot E$, for E less than 6.27 MeV

$J_w \approx 89.57 - 5.917 \cdot E$

$W = 4.1190 + 0.19007 \cdot E$, for E greater than 6.27 MeV

$J_w \approx 21.96 + 4.90 \cdot E$

Reduced Radius

$r_w = 1.3542$

Diffuseness

$a_w = 0.3284 + 0.03822 \cdot E$

Spin-Orbit Potential is the same as give in **Table III-A-1.** (WG86)

Table III-C-1:- Parameters for the elemental rotational coupled-channels model (ROTM) potential. Particle energies (E) and potential strengths (V and W) are given in MeV and geometries in fermis. Approximate strengths in volume-integrals-per-nucleon (J) are in units of MeV-fm^3. These parameters were deduced from measured values at energies of less than 10 MeV, and thus are rigidly valid only below 10-12 MeV...

Real Potential

Strength

$V = 48.218 - 0.33286 \cdot E$

$J_V = 430.16 - 2.9694 \cdot E$

Reduced Radius

$r_v = 1.2446$

Diffuseness

$a_v = 0.6035$

Imaginary Potential

Strength

$W = 2.7928 + 0.34516 \cdot E$

$J_w = 18.27 + 2.2580 \cdot E$

Reduced Radius

$r_w = 1.2934$

Diffuseness

$a_w = 0.4376$

Spin-Orbit Potential is the same as that of **Table III-A-1** (WG86)

Deformations

^{185}Re	$\beta_2 = 0.22$	$\beta_4 = -0.085$
^{187}Re	$\beta_2 = 0.21$	$\beta_4 = -0.085$

Table III-C-2:- Parameters for the ^{187}Re rotational potential (RE187ROT), as described in the text. The nomenclature is the identical to that of **Table III-C-1.**

Real Potential

Strength

$V = 48.934 - 0.3638 \cdot E$

$J_V = 428.2 - 3.184 \cdot E$

Reduced Radius

$r_v = 1.2366$

Diffuseness

$a_v = 0.6011$

Imaginary Potential

Strength

$W = 2.5507 + 0.36422 \cdot E$

$J_w \approx 16.53 + 2.3561 \cdot E$

Reduced Radius

$r_w = 1.2603$

Diffuseness

$a_w = 0.4557$

Spin-Orbit Potential is the same as that of **Table III-A-1** (WG86)

Deformations are same as **Table III-C-1**

Table III-C-3. Correlation of observed inelastic-scattering excitation energies in MeV (Collume A) with reported (**NNDC**) excitations in ^{185}Re (Collume B) and in ^{187}Re (Collume C).

No.	Column A.	Collume B	Collume C
0	0.0	0.0, 5/2+	0.0, 5/2+
1	0.130	0.125, 7/2+	0.134, 7/2+
2	0.214	----------	0.206, 9/2-
3	0.295	0.284, 9/2+	0.303, 9/2+
4	0.386	0.368, 9/2-	0.390, 11/2-
5	0.505	0.475, 11/2+ 0.547, 11/2-	0.511, 1/2+
6	0.635	0.646, 1/2+	0.582, 5/2+ 0.589, 3/2+ 0.618, 3/2+ 0.625, 1/2+ 0.647, 5/2+

-

Table III-C-4:- Parameters for the rotational coupled-channels model (ROTM) potential with smaller β_2 values of 0.190 (^{185}Re) and 0.180 (^{187}Re). Otherwise the nomenclature is identical to that of **Table III-C-1**.

Real Potential

Strength

$V = 48.204 - 0.2746 \cdot E$

$J_V = 420.95 - 2.3980 \cdot E$

Reduced Radius

$r_v = 1.2396$

Diffuseness

$a_v = 0.5949$

Imaginary Potential

Strength

$W = 2.5327 + 0.39296 \cdot E$

$J_w \approx 16.68 + 2.8167 \cdot E$

Reduced Radius

$r_w = 1.2652$

Diffuseness

$a_w = 0.4600$

Spin-Orbit Potential same of **Table III-A-1** (WG86)

Table III-D-1:- Parameters for the SOM potential with dispersion contributions, as described in the text. The nomenclature is identical to that of **Table III-A-1**.

Real Potential

Strength

$V = 43.587 - 0.61101 \cdot E$

Reduced Radius

$r_v = 1.1802$

Diffuseness

$a_v = 0.6549$

Imaginary Potential

Strength

$W = 22.754 - 3.3575 \cdot E$, for E less than 5.72 MeV

$= 1.5256 + 0.35369 \cdot E$, for E greater than 5.72 MeV

Reduced Radius

$r_w = 1.3361$

Diffuseness

$a_w = 0.2742 + 0.03234 \cdot E$

Spin-Orbit Potential the same as given in **Table III-A-1**. (WG86)

Table III-D-2:- Parameters for the rotational potential with dispersion contributions, as described in the text. The nomenclature is identical to that of **Table III-C-1**.

Real Potential

Strength

$V = 48.199 - 0.30699 \cdot E$

Reduced Radius

$r_v = 1.2277$

Diffuseness

$a_v = 0.5768$

Imaginary Potential

Strength

$W = 3.2946 + 0.34156 \cdot E$

Reduced Radius

$r_w = 1.2734$

Diffuseness

$a_w = 0.4217$

Spin-Orbit Potential is the same as that of **Table III-A-1.** (WG86)

Deformations as per **Table III-C-1**.

Fig. II-1. Measured elemental Re differential-scattering cross sections. The experimental values are noted by symbols and curves indicate the results of fitting the measured values with legendre-polynomial expansions. Incident neutron energies, in MeV, are numerically noted. Throughout this work data are presented in the laboratory coordinate system.

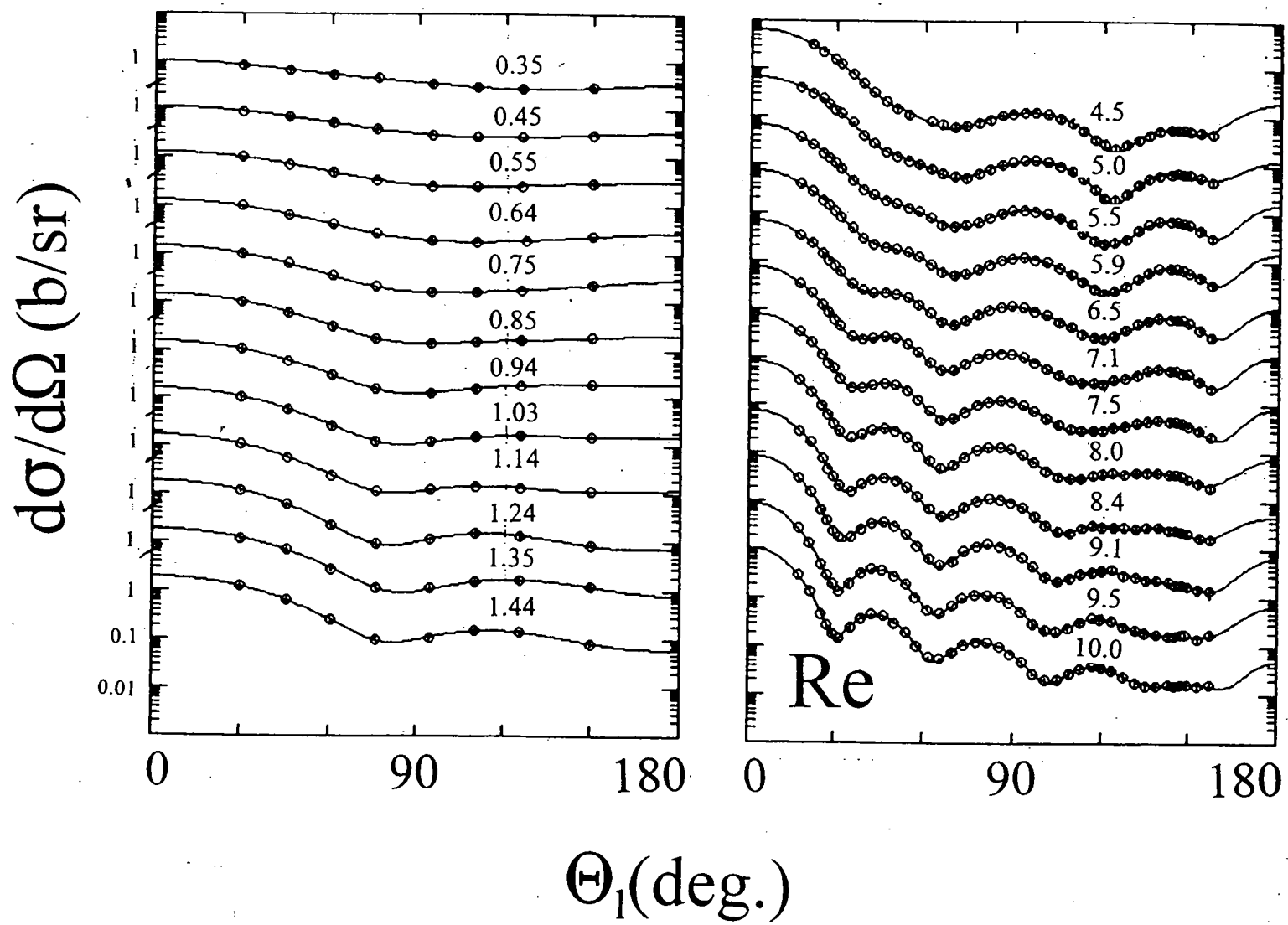

Fig, III-A-1. Comparison of measured (symbols) and SOM-calculated neutron total cross section of elemental rhenium.

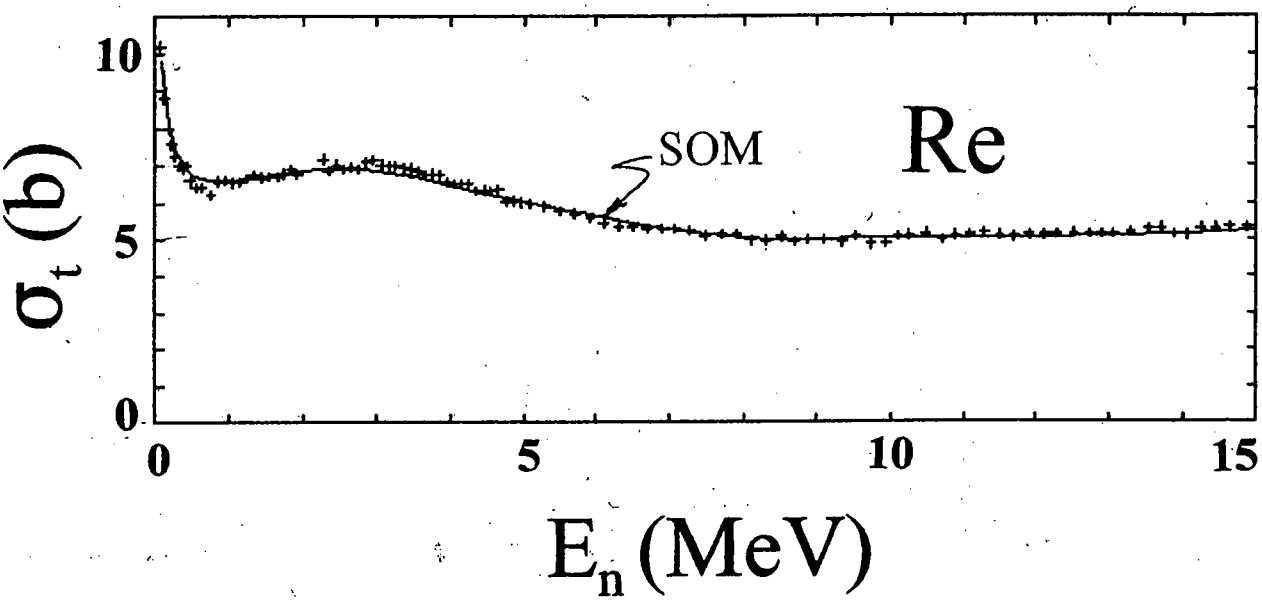

Fig. III-A-2. Comparisons of measured (symbols) and SOM-calculated scattered-neutron "elastic" distributions (curves) of elemental rhenium. Incident-neutron energies are numerically noted in MeV.

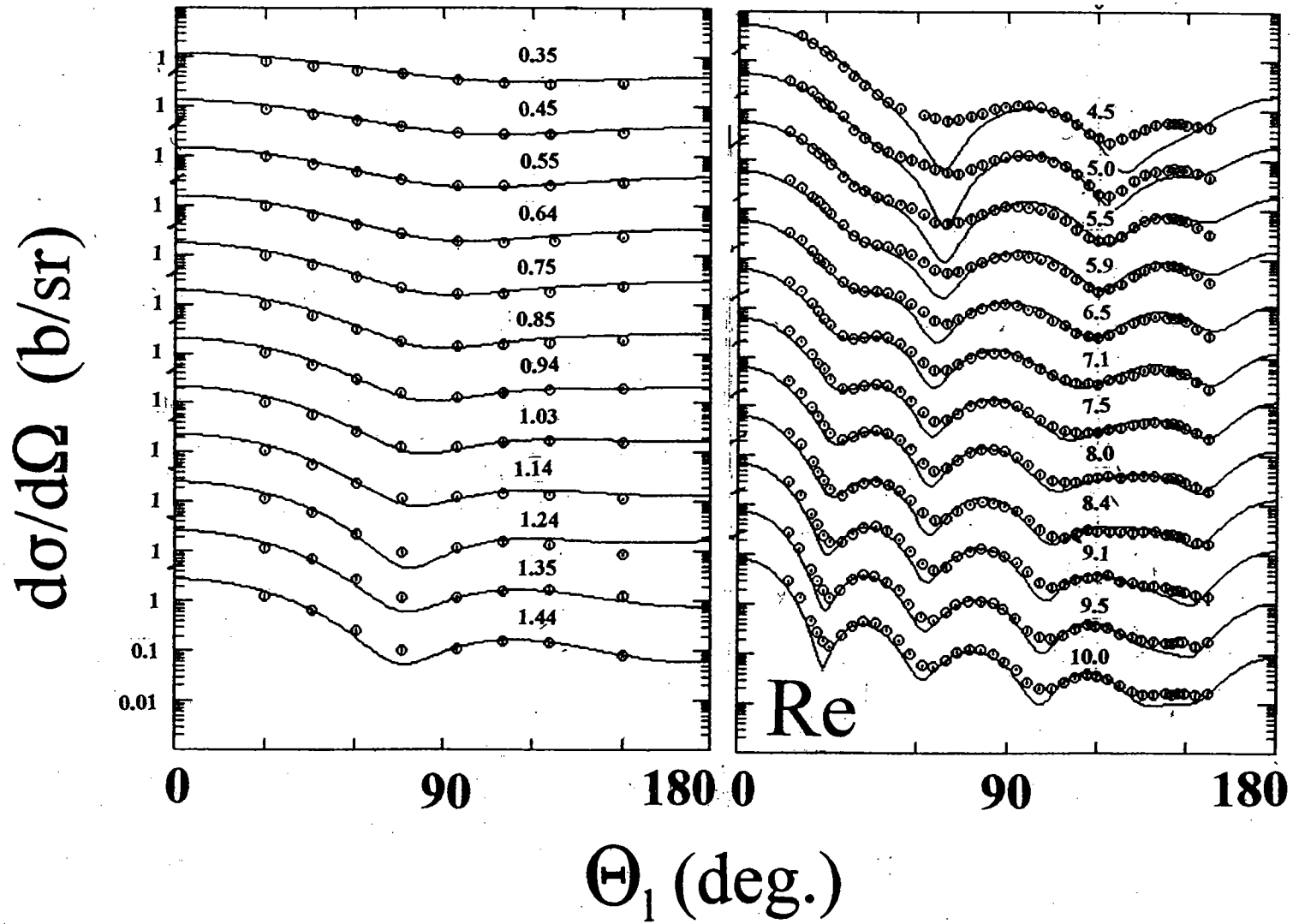

Fig. III-B-1. Measured (symbols) and calculated (curve) total cross sections of elemental rhenium. The calculations are based upon the SOMV potential of **Table III-B-1**. $V_I/W_I = 16/8$ MeV, as per the text.

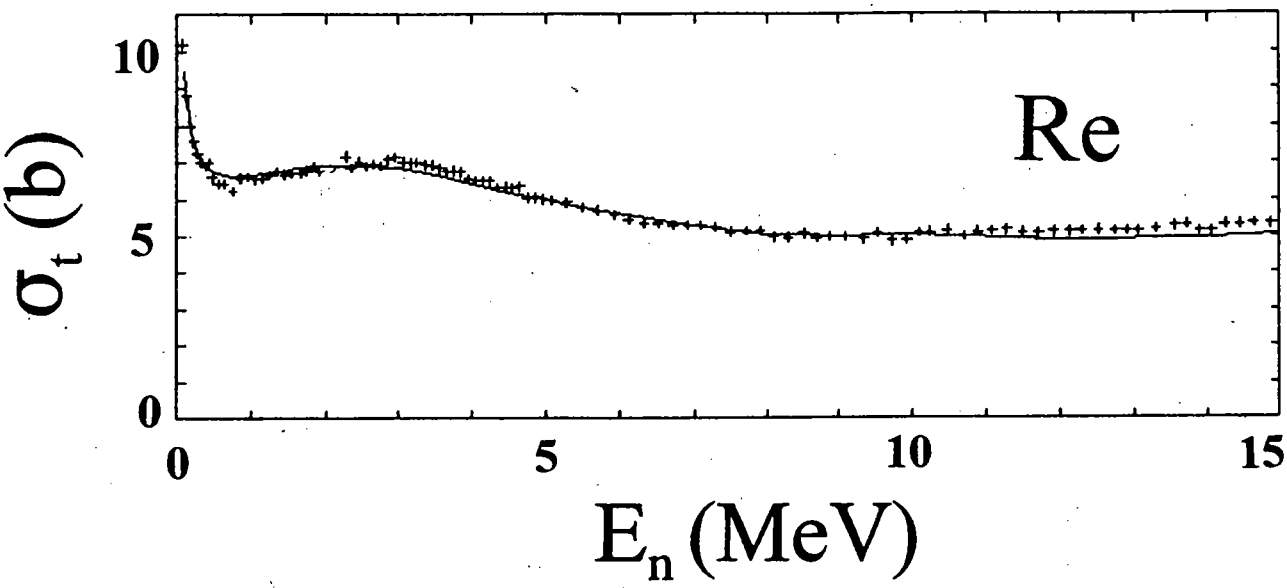

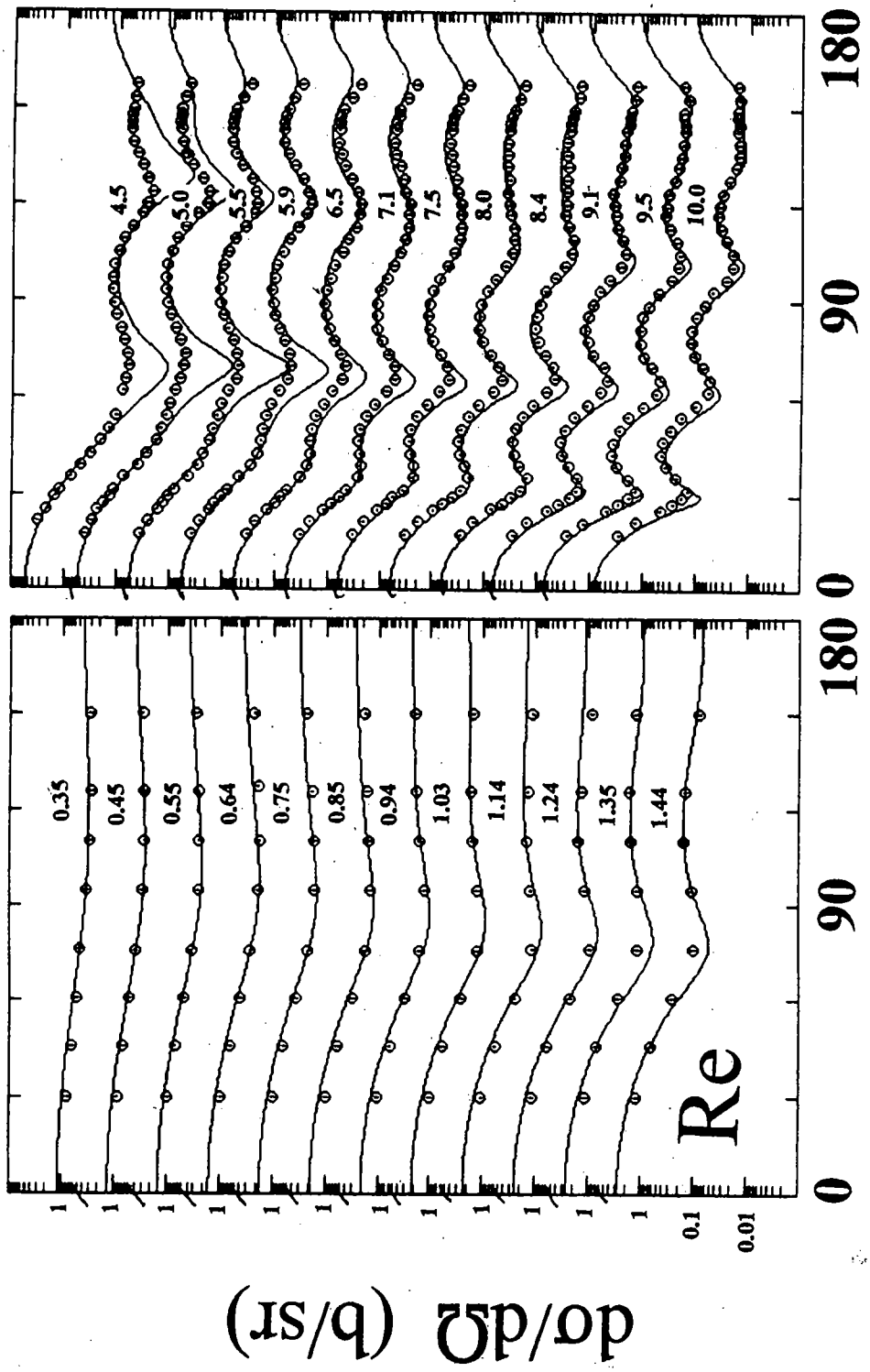

Fig. III-B-2. Measured (symbols) and calculated (curves) differential "elastic" scattering from elemental Re. The calculations used the SOMV potential of **Table III-B-1** with $V_1/W_1 = 16/8$ MeV. The nomenclature is identical to that of **Fig. III-A-2.**

Fig. III-C-1. Comparison of measured (symbols) and ROTM-calculated (curve) neutron total cross section of elemental rhenium. The calculations employed the elemental potential of **Table III-C-1,** as described in the text.

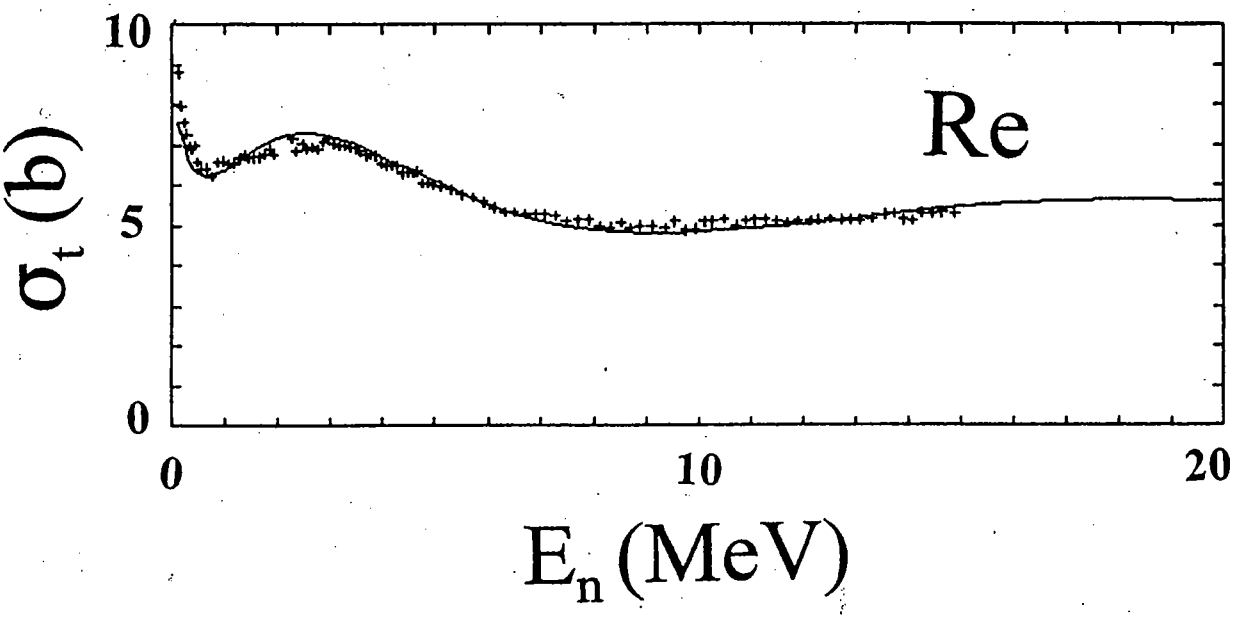

Fig. III-C-2. Comparison of measured (symbols) and calculated (curves) scattering distributions of elemental Rh. The calculations employed the ROTM of **Table III-C-1**. Incident neutron energies are numerically cited. A single curve at a given energy represents simple calculated elastic scattering. At energies with two curves, the elastic (lower) and elastic+first-inelastic excitation of the g.s. rotational band (upper) are represented. At energies with three curves, the first represents simple calculated elastic scattering (lower), the second the elastic+first inelastic distribution, and the third the elastic+the first two inelastic contributions from the g.s. rotational band.

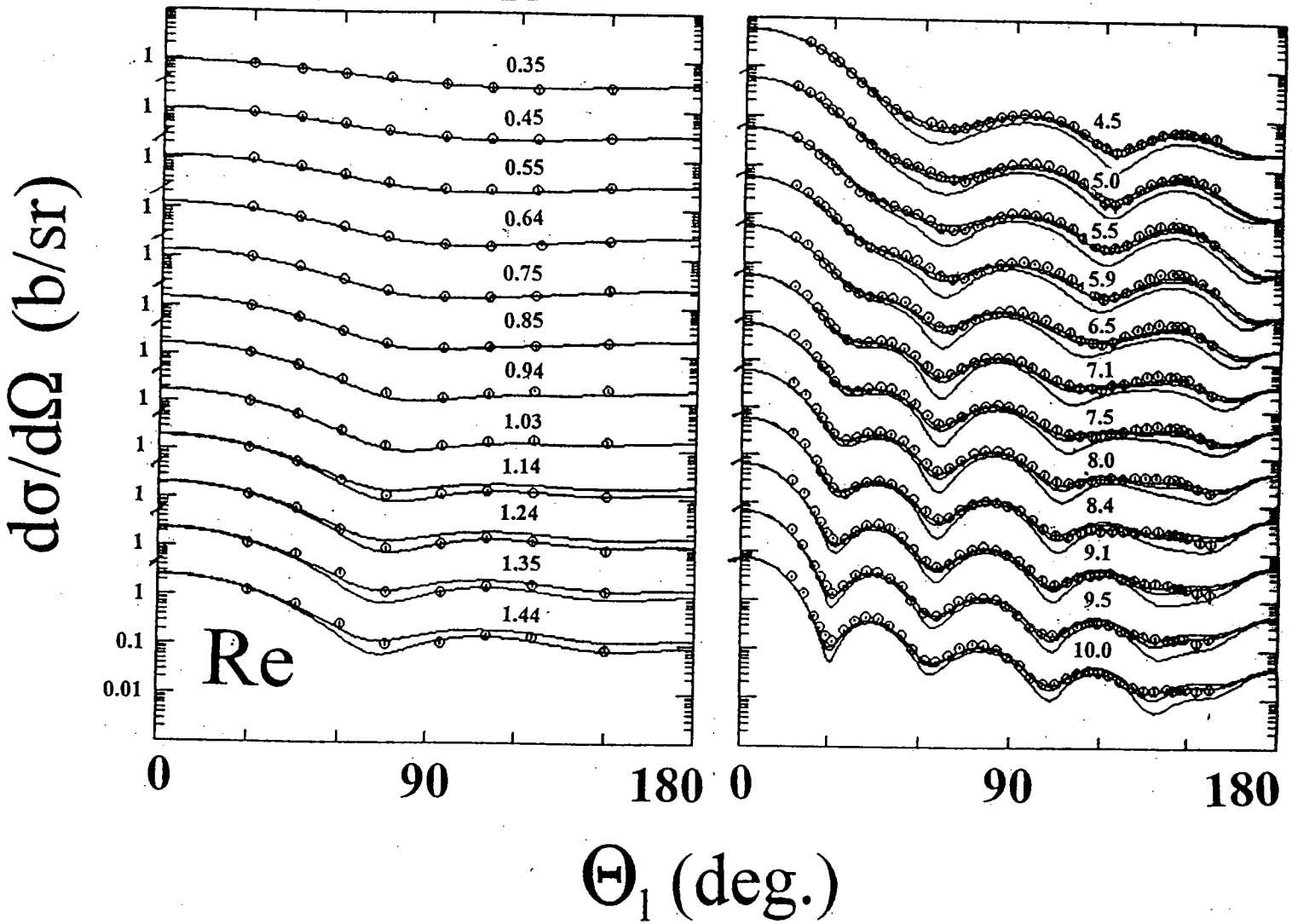

Fig. III-C-3. Comparison of elemental measured (symbols) and calculated total cross sections (curves) of ^{187}Re. The calculations employed the parameters of **Table III-C-2.**

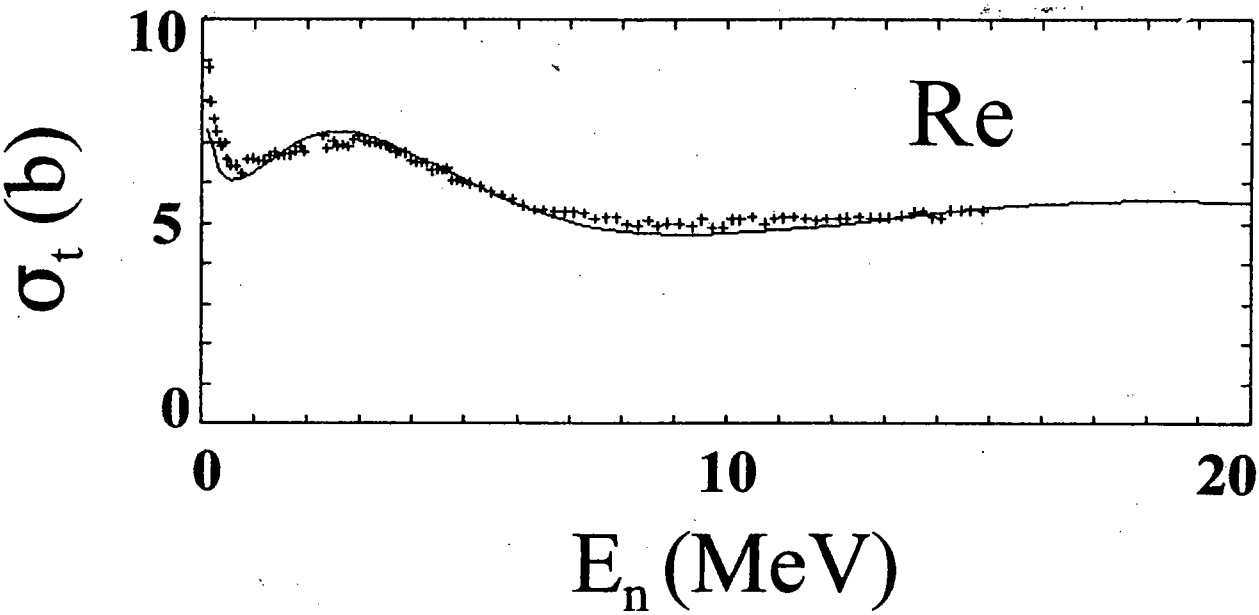

Fig. III-C-4. Comparison of elemental measured (symbols) and calculated (curves) differential-scattering cross sections of ^{187}Re. The calculations employed the potential of **Table III-C-2.** The nomenclature is identical to that of **Fig. III-C-2.**

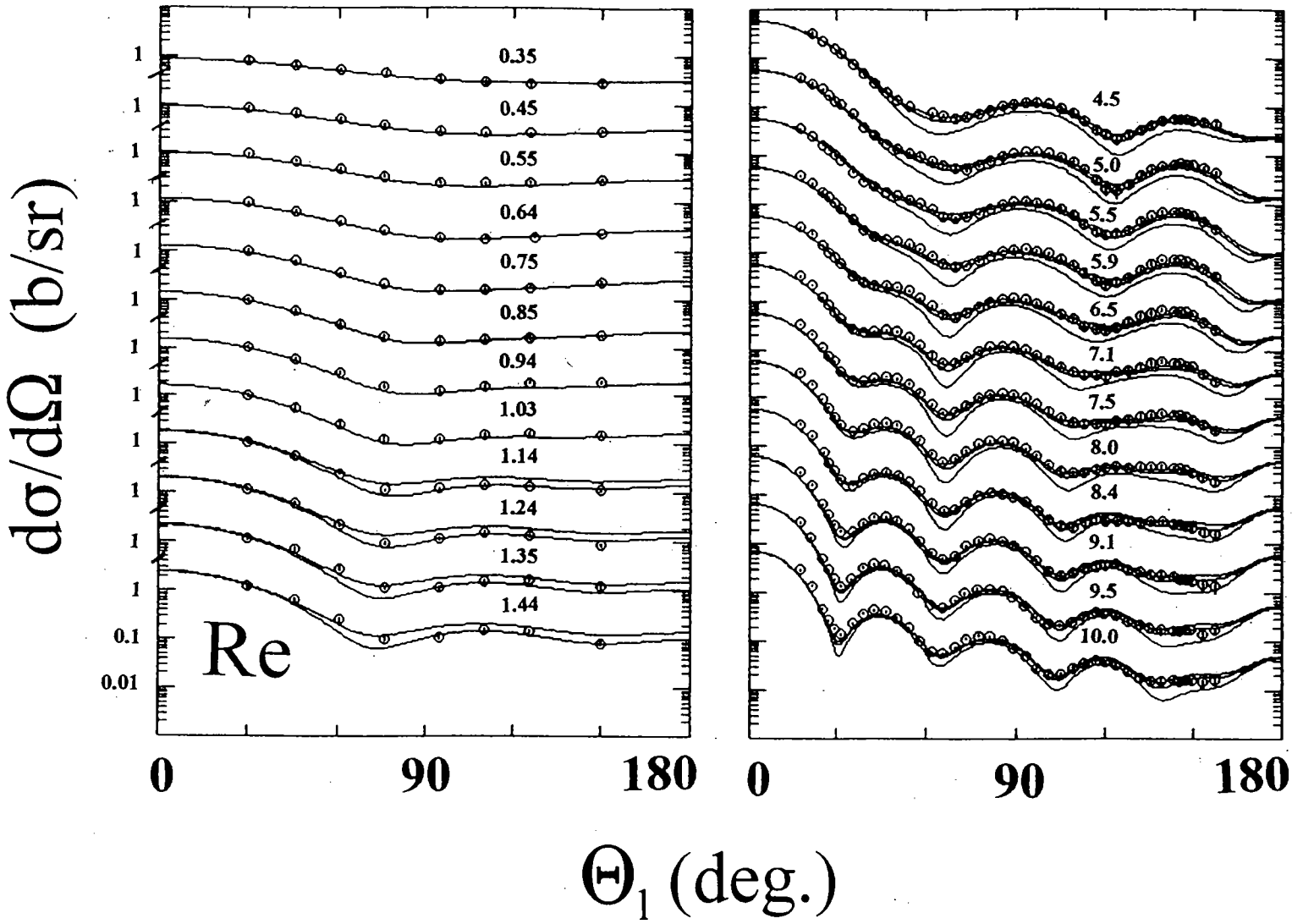

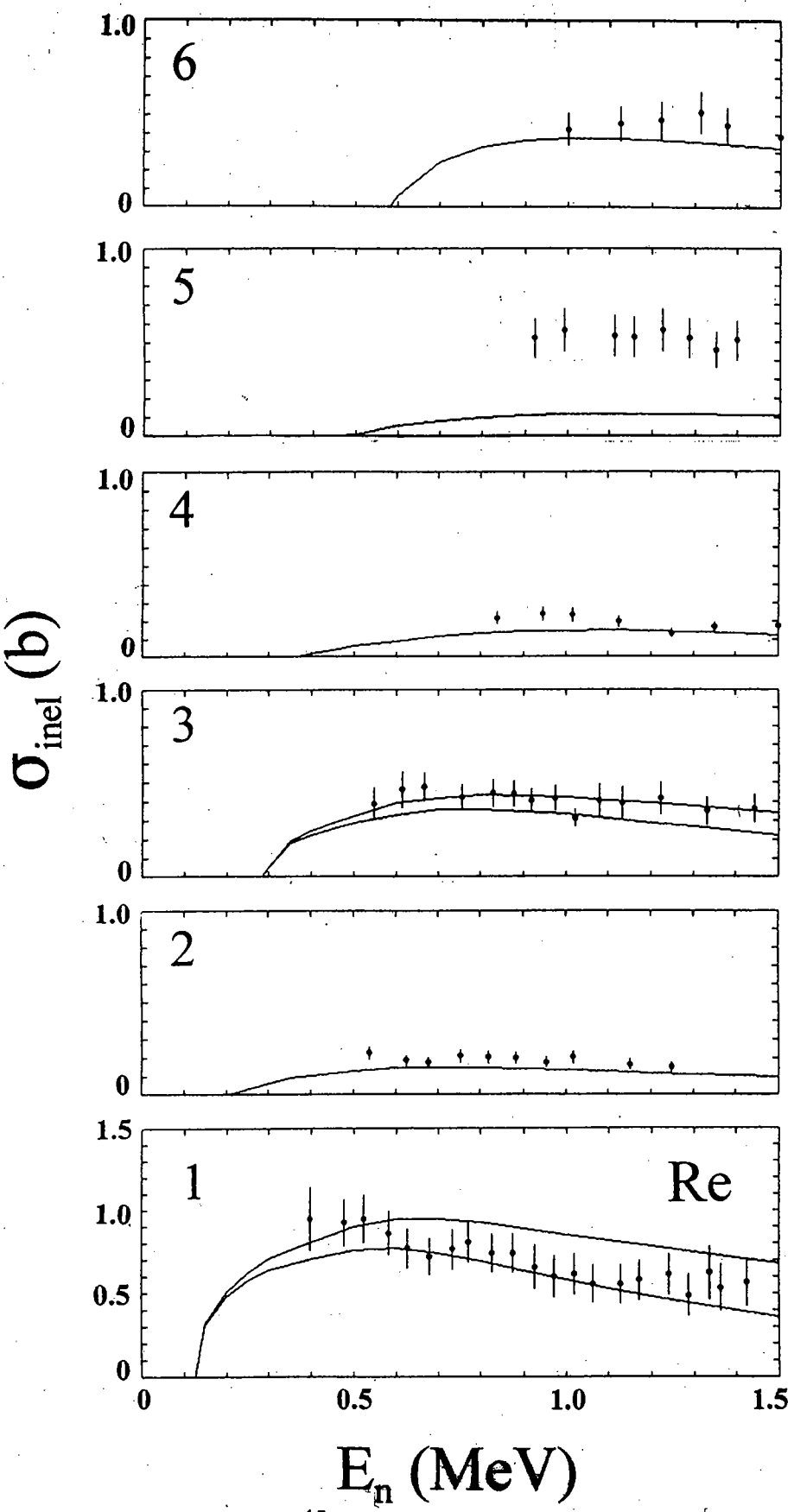

Fig. III-C-5. Measured (symbols) and calculated (curves) inelastic-excitation cross sections of elemental rhenium. The calculations were based upon the ROTM potential of **Table III-C-1.** The excitation energies 1 through 6 are correlated with reported level structure in the two isotopes of rhenium in **Table III-C-3.**

Fig. III-C-6. Comparison of measured (symbols) and calculated (curve) cross sections for the inelastic neutron excitation of the first excited levels in the two isotopes making up elemental rhenium. The calculations used the reduced deformations and parameters of **Table III-C-4**, as discussed in the text.

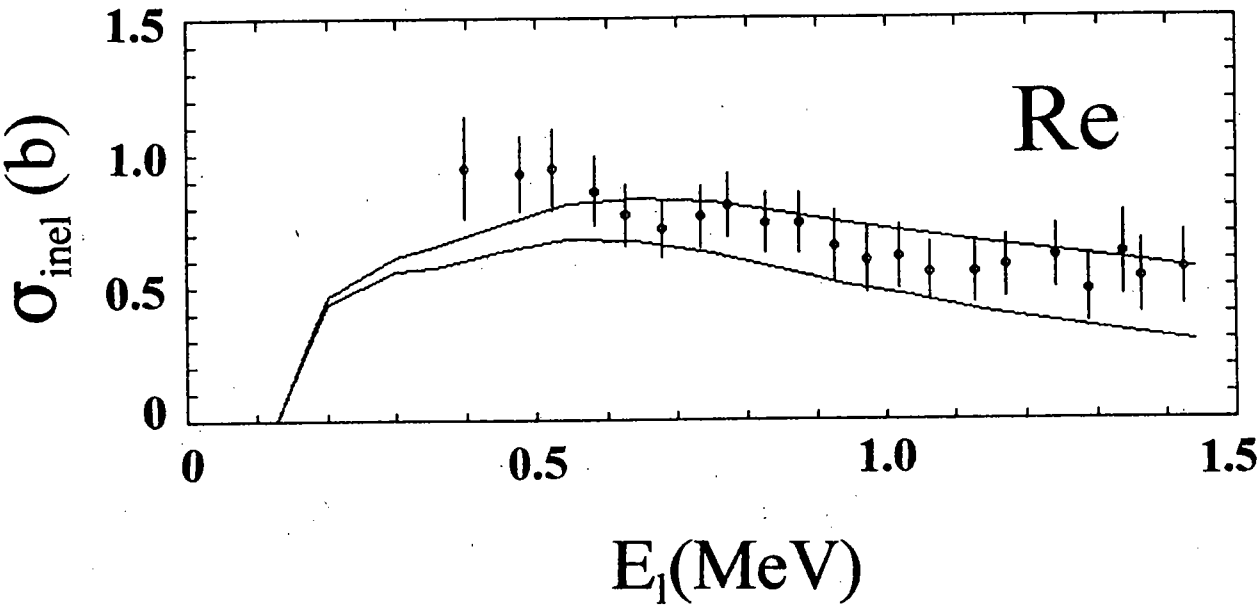

Fig. III-C-7. Comparison of measured (symbols) and calculated (curves) differential "elastic"-scattering distributions of elemental rhenium. The calculations used the parameters and reduced deformations of **Table III-C-4.**

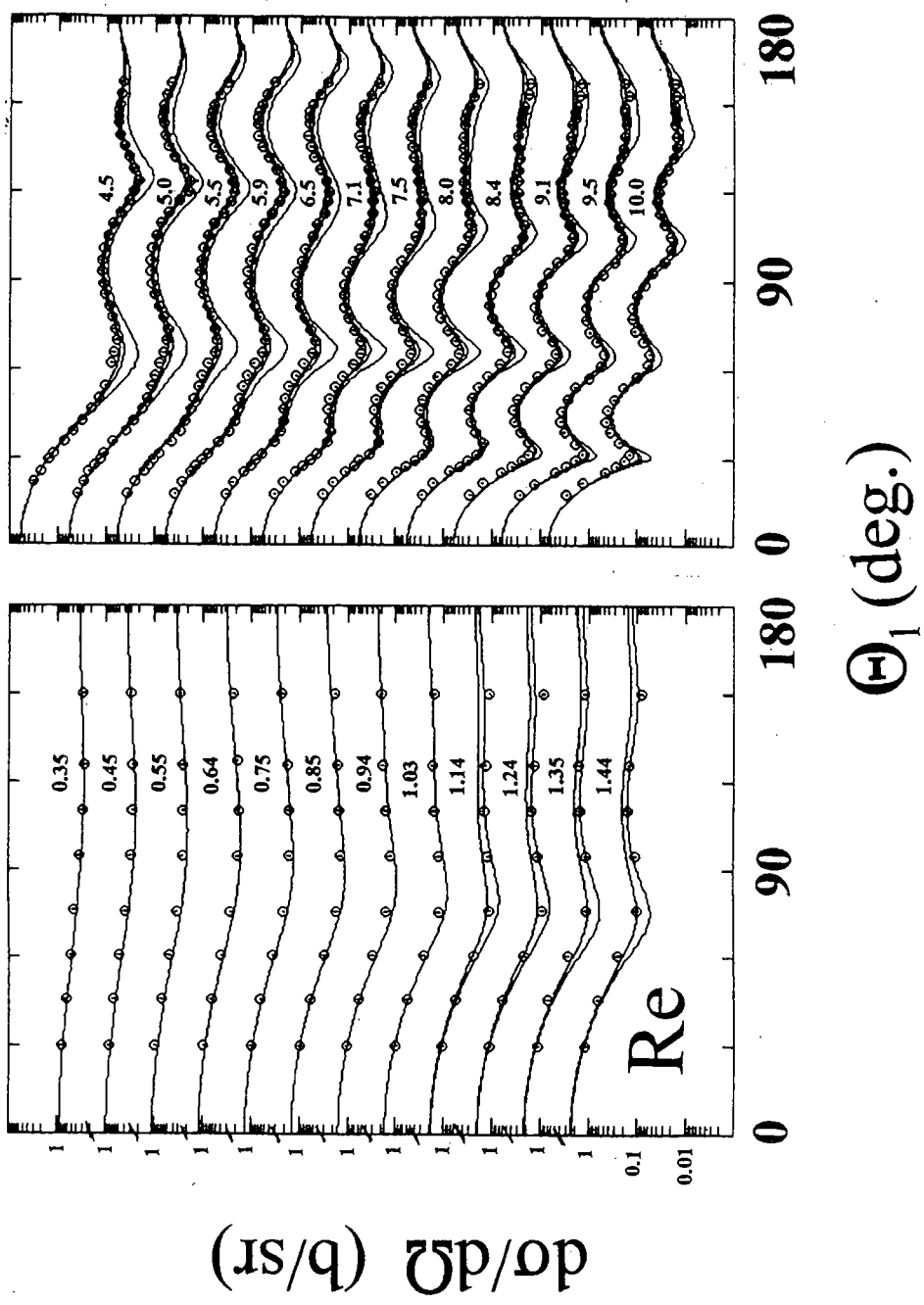

Fig. III-D-1. The fraction of the imaginary potential strength (DISP) that will be reflected into the real potential. These are the values of the ratio $\Delta J_{sur}/J_w$ of **Eq. III-D-2** as a function of energy.

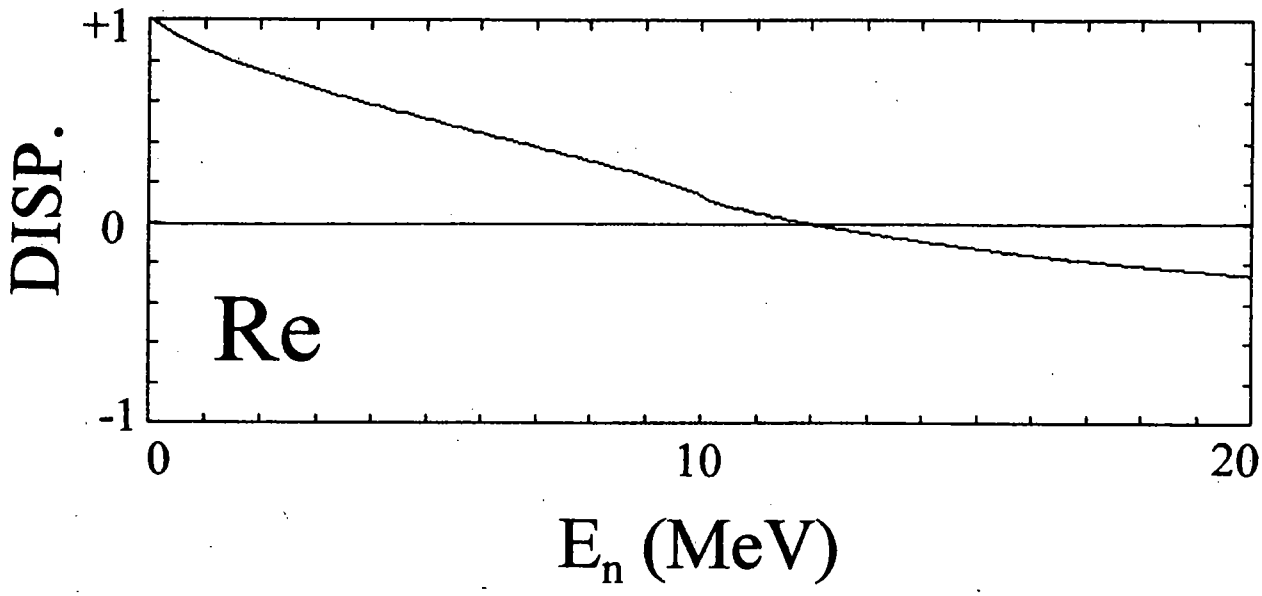

Fig. III-D-2. Comparison of measured (symbols) and calculated (curve) total cross sections of elemental rhenium. The calculations used the spherical dispersive potential of **Table III-D-1.**

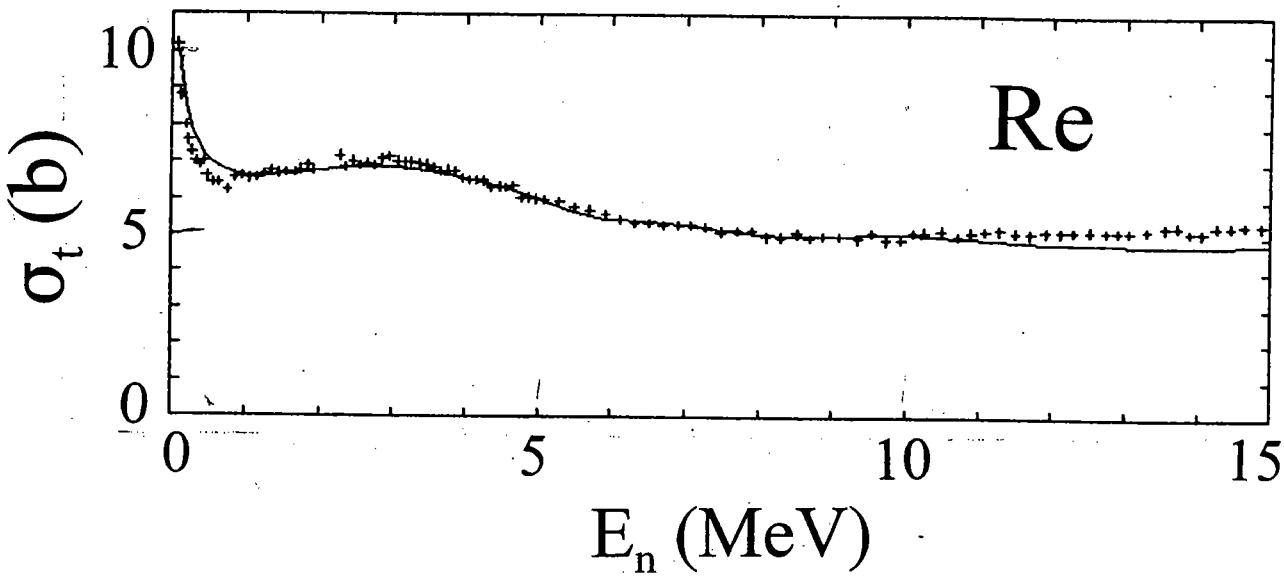

Fig. III-D-3. Comparison of measured (symbols) and calculated (curves) differential "elastic" scattering cross sections of elemental rhenium. The calculations used the spherical dispersive potential of **Table III-D-1.** The nomenclature is the same as **Fig. III C-2.**

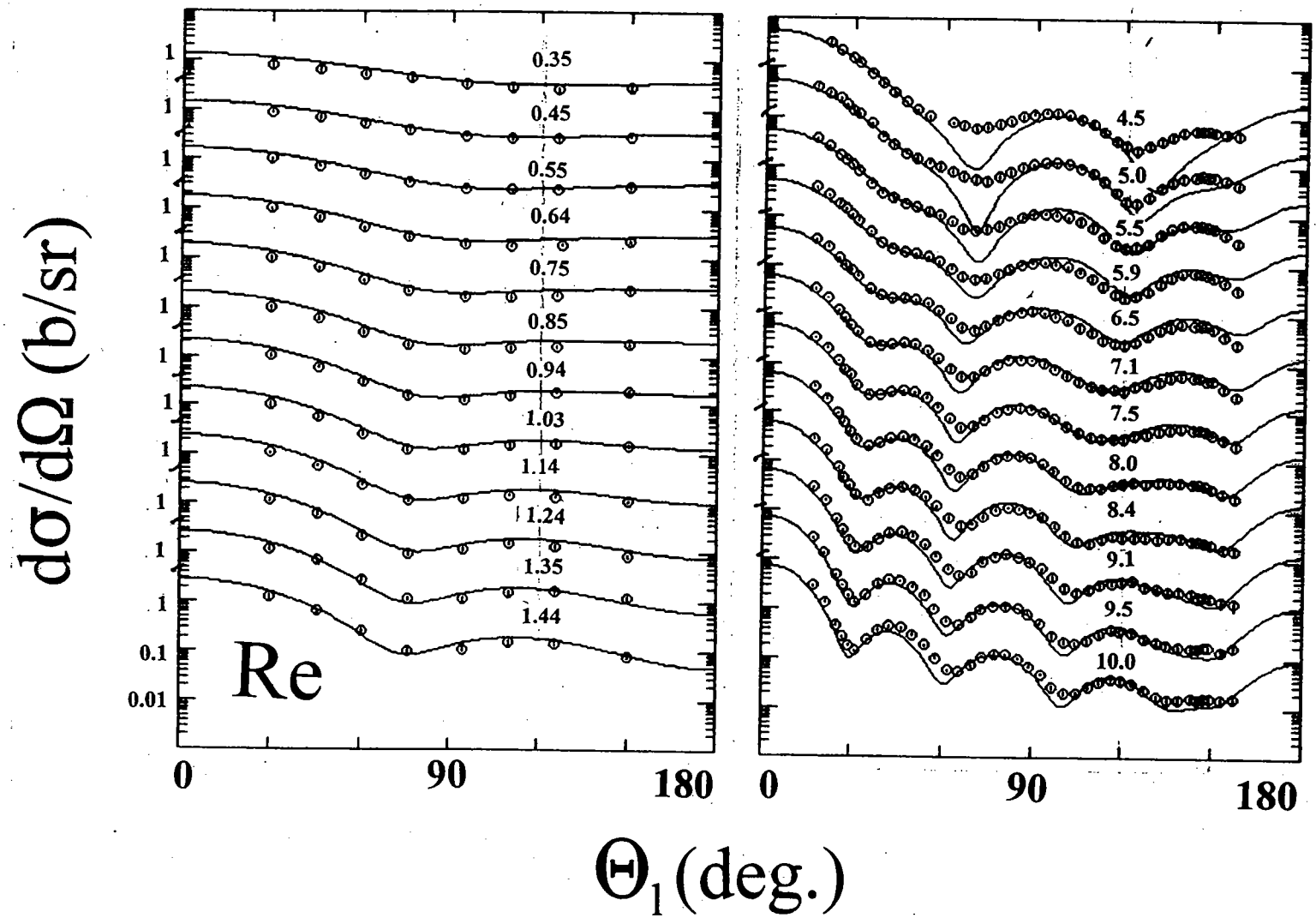

Fig. III-D-4. Comparison of measured (symbols) and calculated (curve) total cross section of elemental rhenium. The calculations used the rotational potential of **Table III-D-2,** including dispersive effects.

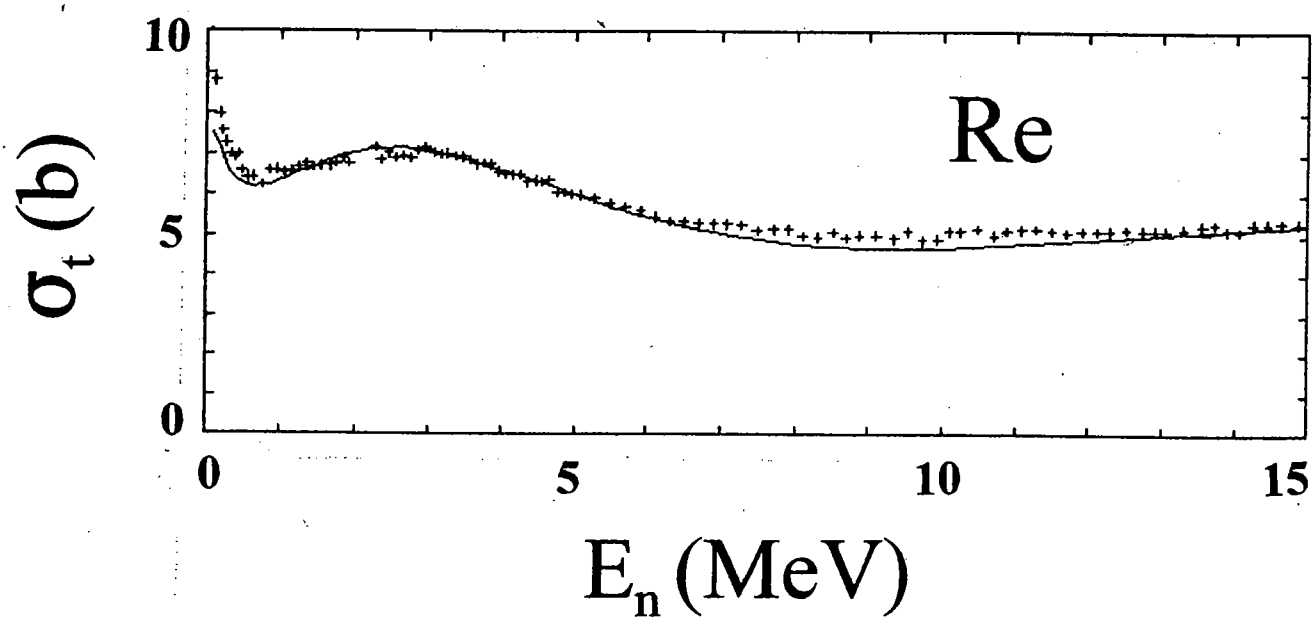

Fig. III-D-5. Comparison of measured (symbols) and calculated (curves) differential "elastic" scattering of elemental rhenium. The calculations used the rotational potential of **Table III-D-2** including dispersive effects. Otherwise, the nomenclature of the figure is identical to that of **Fig. III-C-2.**

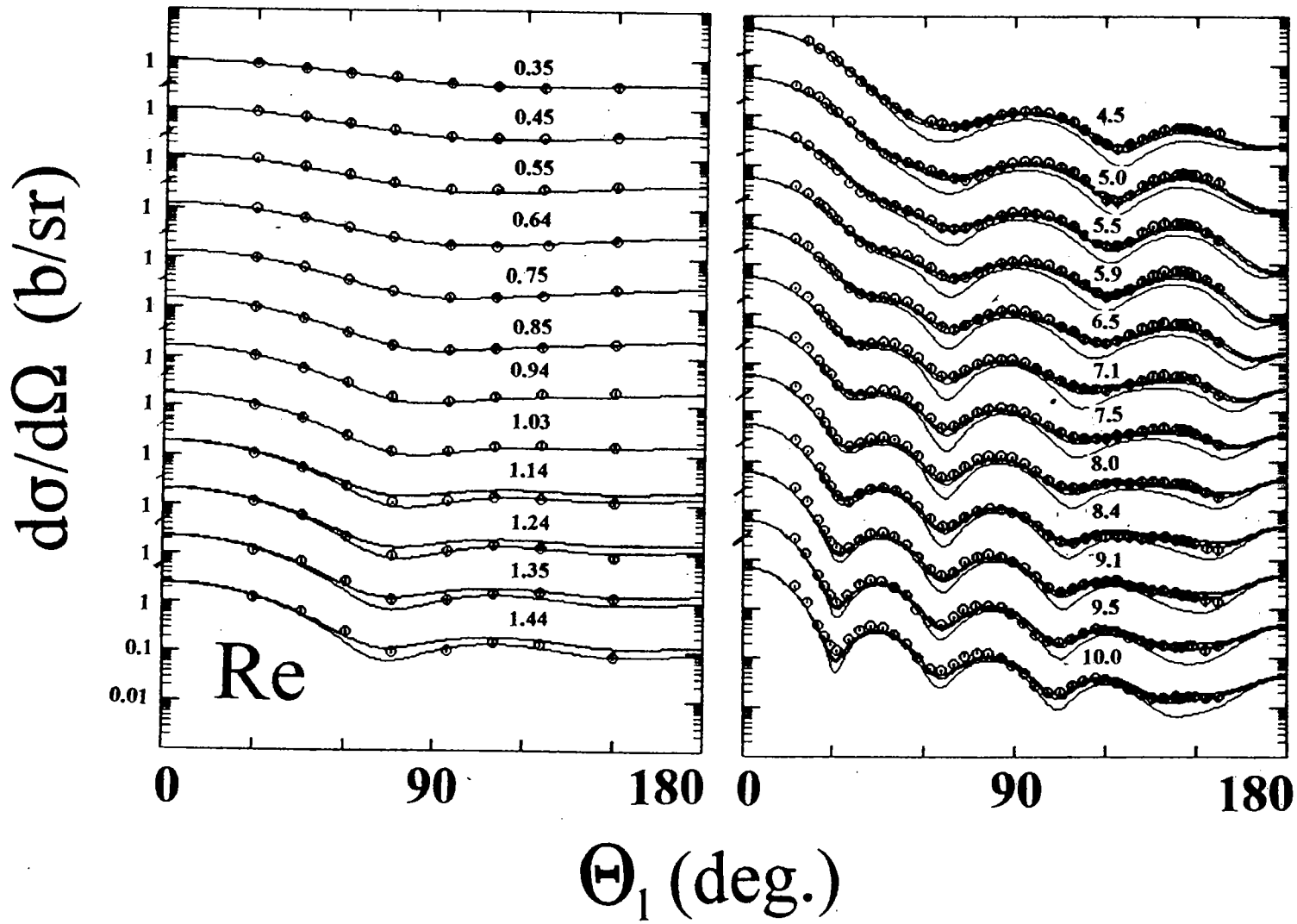

Fig. V-A-1. Illustrative comparisons of measured (symbols) and calculated (curves) neutron total cross sections of elemental rhenium. Sections A to E of the figure correspond to potential variants defined and discussed in the text.

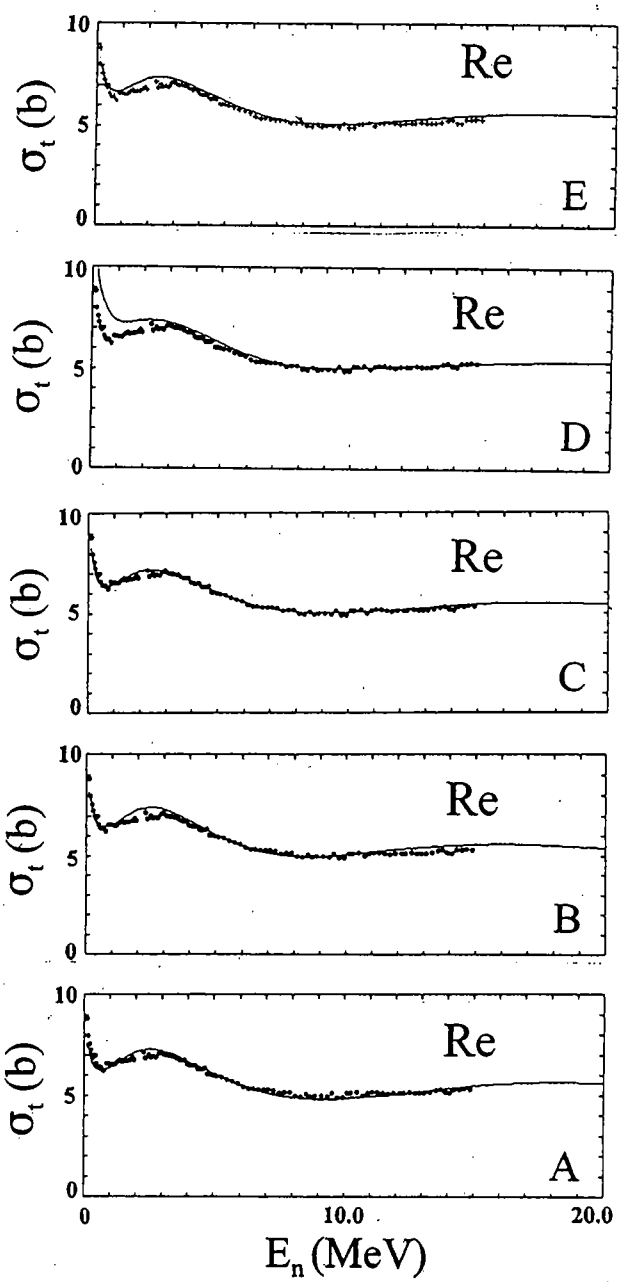

Fig. V-A-2. Comparisons of measured (symbols) and calculated (curves) differential-scattering distributions. Panels A through E correspond to the potentials defined and discussed in the text. The nomenclature of the figure is identical to that of **Fig. III-C-2**.

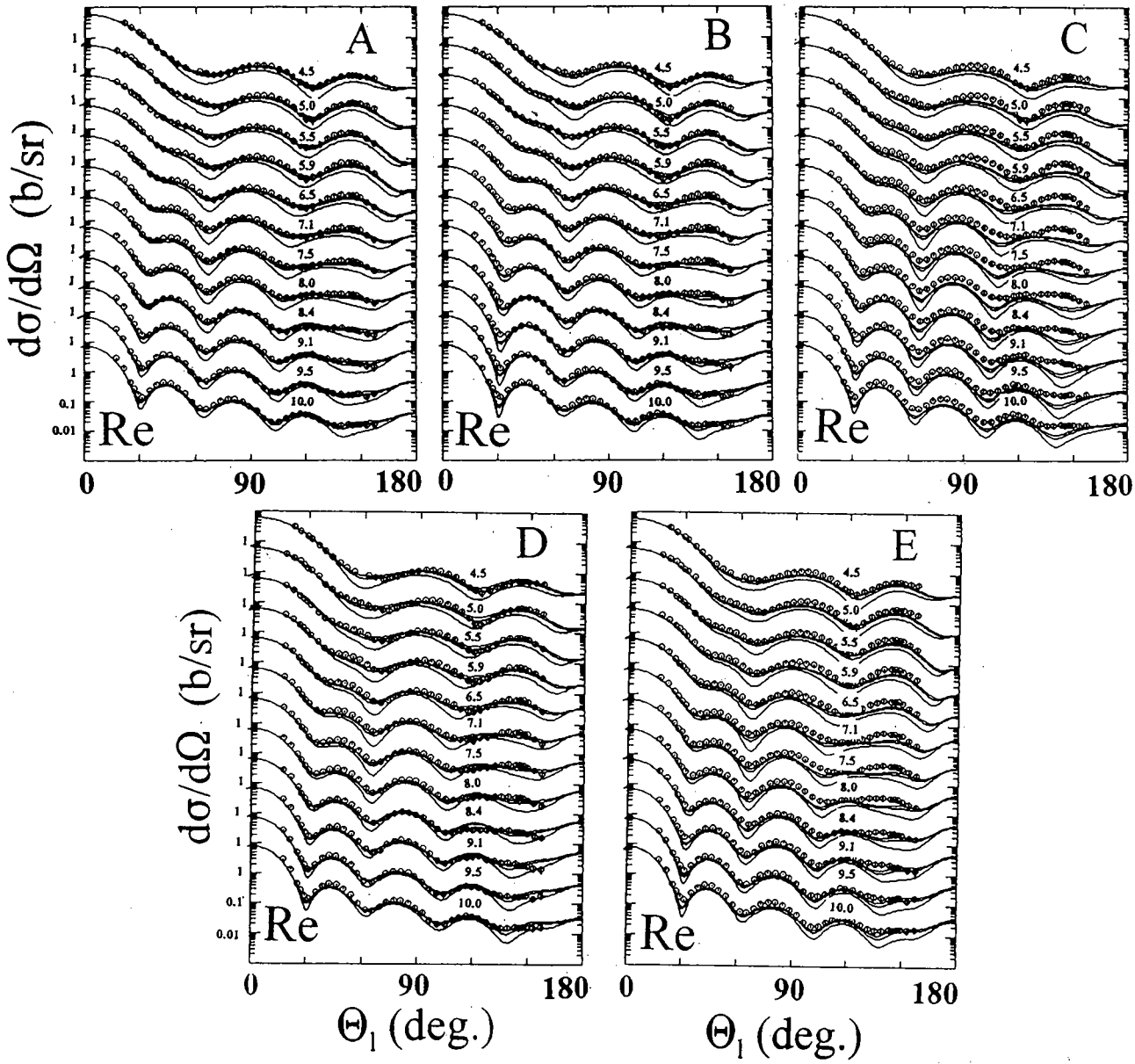

Fig. V-B-1. Comparison of measured ("+" symbols), calculated (with the ROTM, curve with "x" symbols), and ENDF/B-VI evaluated (curve with "o" symbols) neutron total cross sections of elemental rhenium.

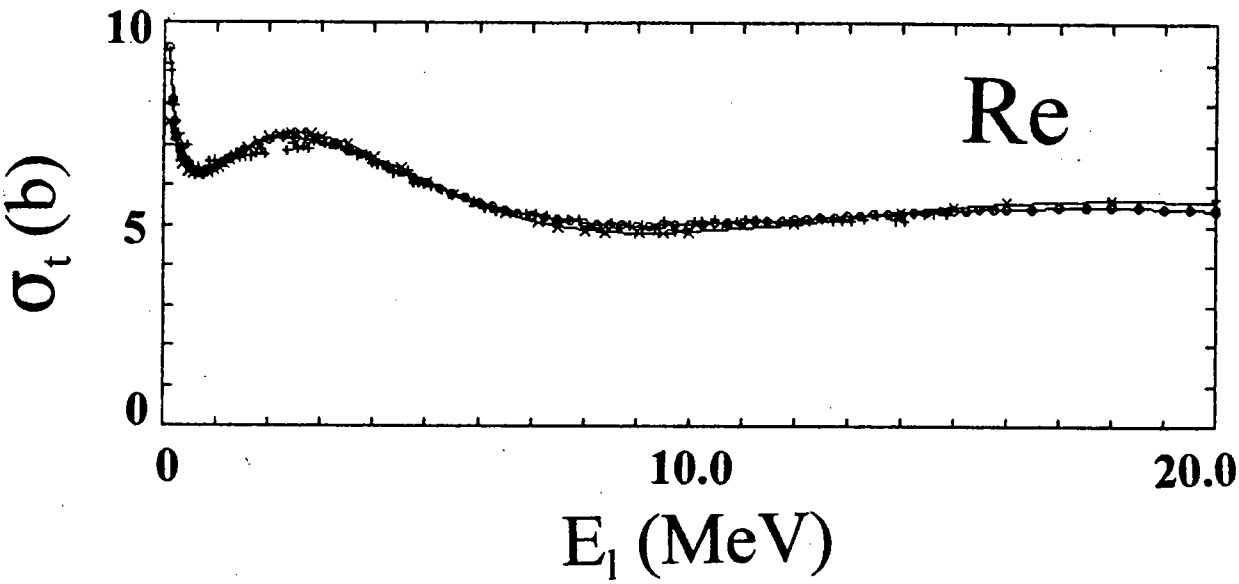

Fig. V-B-2. Upper panel:- Comparison of evaluated and calculated elastic-scattering cross sections of ^{185}Rh. The curve with "x" symbols indicates the results of ROTM calculations, while the curve with "o" symbols denotes the ENDF/B-VI evaluation. The middle panel is the same as the upper panel, but referenced to the ^{187}Re isotope. The lower panel compares the experimental results (symbols) of this work for the inelastic excitation of the first excited level of the g.s. rotational band with the elemental results implied by the ENDF/B-VI isotopic files (curve).

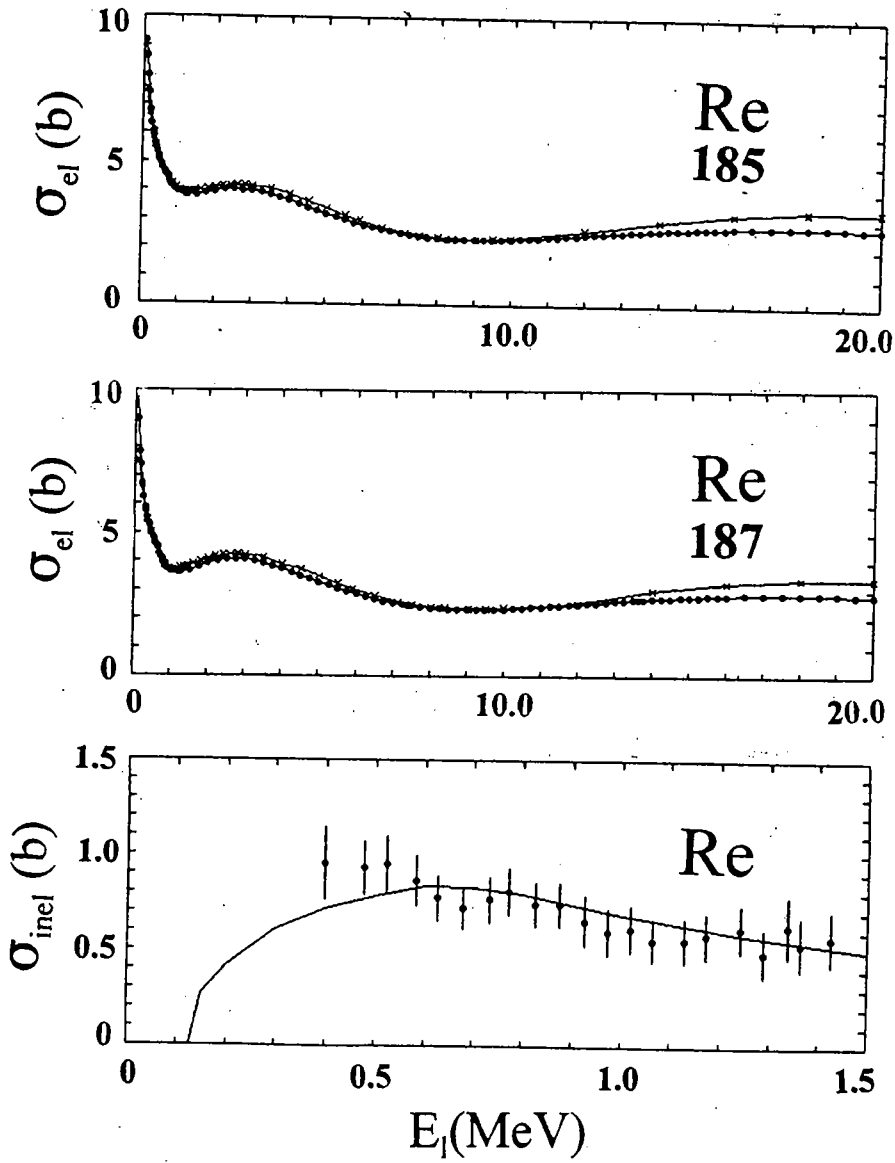

Fig. A-1. The elemental rhenium total cross section data base (symbols) and the END/B-VI evaluation (curve).